Electronic Supplementary Material (ESI) for Journal of Materials Chemistry C.

Supporting Information

A facile color-tuning strategy for constructing a library of Ir(III) complexes with fine-tuned phosphorescence from bluish green to red using synergetic substituent effect of $–OCH_3$ and –CN at merely the C-ring of C^N ligand

Yan Jiao,‡[a] Ming Li,‡[a] Ning Wang,[a] Tao Lu,[a] Liang Zhou,*[b] Yan Huang,[a] Zhiyun Lu,*[a] Daibing Luo[c] and Xuemei Pu*[a]

[a.]Key Laboratory of Green Chemistry and Technology (Ministry of Education), College of Chemistry, Sichuan University, Chengdu 610064, PR China

*E-mail: xmpuscu@scu.edu.cn; Fax: +86-28-85412907. luzhiyun@scu.edu.cn;

Fax: +86-28-85410059.

[b.]State Key Laboratory of Rare Earth Resource Utilization, Changchun Institute of Applied Chemistry, Chinese Academy of Sciences, Changchun 130022, PR China

*E-mail: zhoul@ciac.ac.cn.

[c.]Analytical and Testing Centre, Sichuan University, Chengdu, 610064, PR China

‡These authors contributed equally to this work.

Experimental section

General Information

All the reagents involved in the synthetic procedure were commercially available and used without further purification unless otherwise stated. All the solvents were of analytical grade and freshly distilled prior to use. Anhydrous tetrahydrofuran and dichloromethane were prepared by freshly distilling over sodium/benzophenone and diphosphorouspentoxide, respectively, under a nitrogen atmosphere. ^{1}H NMR and ^{13}C NMR spectra were measured on a Bruker AVANCE-400 spectrometer in $CDCl_3$ or DMSO-d_6 using TMS as the internal standard. High resolution MS spectra were obtained from a Q-TOF Priemier ESI mass spectrometer (Micromass, Manchester, UK). The crystallographic data for **4d**~**4g** reported here have been deposited in the Cambridge Structural Database (CCDC 1417108, 1417110, 1417109, and 1417111). Single crystal X-ray diffraction data of the complexes were obtained on a X calibur E X-ray single crystal diffractometer equipped with graphite monochromator Mo-Kα (λ = 0.71073 Å) radiation. The data collection was executed using CrysAlisPro program.[1] The structures were determined using direct method and successive Fourier difference syntheses (SHELXS-97) and refined using full-matrix least squares procedure on F^2 with anisotropic thermal parameters for all non-hydrogen atoms (SHELXL-97). Thermogravimetric analysis (TGA) was performed on a TGA Q500 instrument under nitrogen atmosphere at a heating rate of 10 °C min^{-1}. PL emission spectra of both solution and thin-film samples were recorded on a Perkin-Elmer LS55 fluorescence spectrophotometer at 298 K. UV-Vis absorption spectra were measured on a Hitachi U-4100 UV-Vis-NIR scanning spectrophotometer. The concentration of solution samples for PL measurements was 5×10^{-6} mol L^{-1} (in CH_2Cl_2). Relative PL quantum yields (PLQYs) of the solution samples were carried out at room temperature in argon degassed 5×10^{-6} mol L^{-1} CH_2Cl_2 solution, using *fac*-Ir(ppy)$_3$ (φ_{PL} = 0.73 in toluene) as the reference compound under excitation of 400 nm.

The absolute PLQYs of the film samples with the complexes as dopant (doping-level: 5 wt%) and TCTA as the matrix were determined with an integrating sphere (IS80 from Labsphere) together with a digital photometer (S370 from UDT) under ambient conditions. All the film samples were obtained by spin-coating from their corresponding chloroform solutions with concentration of 10 mg mL^{-1} at a speed of 1000 rpm for 40 s on quartz substrates. Cyclic voltammetry (CV) measurements were carried out in argon-purged 5×10^{-4} mol L^{-1} anhydrous CH_2Cl_2 solution with 0.1 mol L^{-1} tetrabutylammonium perchlorate as the supporting electrolyte at a scanning rate of 100 mV s^{-1} using a PARSTAT 2273 electrochemical workstation. The CV system was constructed using platinum plate, $Ag/AgNO_3$ (0.1 mol L^{-1} in acetonitrile) electrode and platinum wire as the working electrode, quasi-reference electrode and counter electrode, respectively. Each measurement was calibrated with a ferrocene/ferrocenium (Fc/Fc^+) redox couple as the external standard.

Computational method

The ground state (S_0) geometries of complexes **4a**~**4g** were fully optimized using B3LYP[2] hybrid functional of density functional theory (DFT). Vibrational frequencies were calculated at the same theoretical level to confirm that each configuration is a true minimum on the potential energy surface. Based on the optimized geometries, the absorption and emission properties were calculated by time-dependent density functional theory (TD-DFT)[3] with B3LYP method. In all calculations, the 6-31G* basis set was used for non-metal atoms while a "double-ζ" quality basis set LANL2DZ[4] along with the pseudo potential was employed for the iridium atom. All calculations above were performed using the program of Gaussian 09 software package[5] and included CH_2Cl_2 solvent environment using the polarizable continuum model (PCM).[6]

OLED fabrication and measurements

The carrier-transporting and host materials for fabrication of OLEDs were obtained commercially and used as received without further purification. Indium-tin-oxide (ITO) coated glass with a sheet resistance of 15 Ω sq^{-1} was used as the anode substrate. Prior to film deposition, pre-patterned ITO substrates were cleaned with detergent, rinsed in de-ionized water, dried in an oven, and finally treated with oxygen plasma for 10 minutes at a pressure of 10 Pa to enhance the surface work function of ITO anode (from 4.7 to 5.1 eV).[7] All the organic layers were deposited with the rate of 0.1 nm s^{-1} under high vacuum ($\leq 3 \times 10^{-5}$ Pa). The light-emitting layers were prepared by co-evaporation of the guest and host materials from two individual sources, and the doping concentrations were modulated by controlling the evaporation rate of the dopant and host. LiF and Al were deposited in another vacuum chamber ($\leq 8.0 \times 10^{-5}$ Pa) with the rates of 0.01 and 1 nm s^{-1}, respectively, without being exposed to the atmosphere. The thickness of these deposited layers and the evaporation rate of different materials were monitored in vacuum with quartz crystal monitors. A shadow mask was used to define the cathode so that the emission area of the devices is 9 mm^2. Current density-voltage-luminance (*J-V-L*) characteristics of the devices were measured by using a programmable Keithley source measurement unit (Keithley 2400 and Keithley 2000) with a silicon photodiode. EL spectra were obtained with a calibrated Hitachi F-7000 fluorescence spectrophotometer.

Synthesis

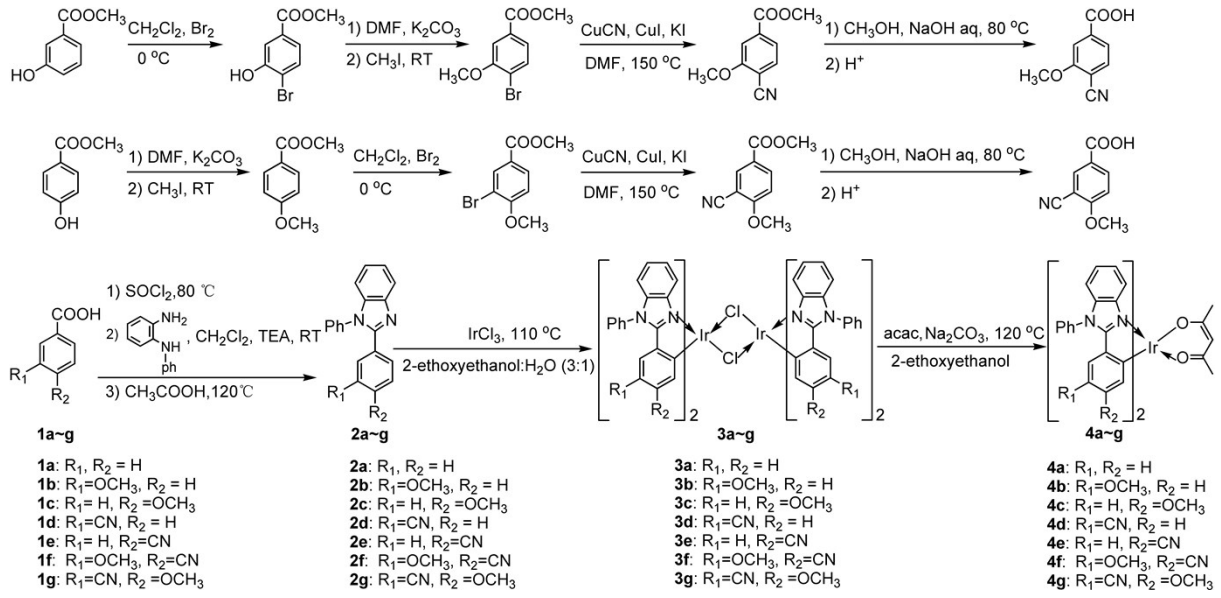

Scheme S1. Detailed synthetic procedures to the Ir(III) complexes **4a-4g**.

The synthetic routes to complexes **4a**~**4g** are shown in Scheme S1. Complex **4a** was prepared according to the literature report.[8] The reactants of 3-cyanobenzoic acid (**1d**) and 4-cyanobenzoic acid (**1e**) were purchased from Aldrich Co., and used without further purification. The intermediates 3-methoxybenzoic acid (**1b**) and 4-methoxybenzoic acid (**1c**) were synthesized according to literature report.[9] The intermediates 4-cyano-3-methoxybenzoic acid (**1f**) and 3-cyano-4-methoxybenzoic acid (**1g**) were synthesized by bromation of methyl 3-hydroxybenzoate or methyl 4-methoxygbenzoate, cyanation through Rosenmund-von Bran reaction,[10] followed by hydrolysis reaction. The detailed synthetic routes to **1f** and **1g** are illustrated in Scheme S1.

Synthesis of 4-cyano-3-methoxybenzoic acid (1f)

To a 100 mL three-necked flask was added methyl 3-hydroxybenzoate 3 g (19.7 mmol) and 30mL of dichloromethane, then 1.1 mL (21.7 mmol) of bromine was added dropwise at 0 °C under stirring for 6 h. Then the reaction was quenched by adding 30 mL of saturated aqueous $NaHSO_3$ under stirring. The reaction mixture

was extracted with ethyl acetate (30 mL × 3), the organic layers were combined and washed with water and brine, then dried over anhydrous Na_2SO_4. After the solvent was removed, the crude product was purified by column chromatograph over silica using petroleum ether/dichloromethane (1/1) as eluent to obtaine methyl 4-bromo-3-hydroxybenzoate as white solid. Yield: 39.6%, m.p.:121-123°C.

To a 100 mL three-necked flask was added methyl 4-bromo-3-hydroxybenzoate 4.5 g (19.5 mmol), anhydrous potassium carbonate 27 g (197 mmol) and 30mL of DMF, then the reactant was stirred at 50°C for 4 h. After the reaction mixture was cooled down to 0°C, 3.6 g of methyl iodide (20.5 mmol) was added dropwise, followed by stirring at RT for 10 h. The reaction mixture was poured into 150 mL of water, then was extracted with with ethyl acetate (30 mL × 3). The organic layers were combined and washed with water and brine, then dried over anhydrous Na_2SO_4. After the solvent was removed, the crude product was recrystallized from methanol to afford methyl 4-bromo-3-methoxybenzoate as a white solid. Yield: 91%, m.p.: 76-78°C. ^{1}H NMR (400 MHz, $CDCl_3$) δ(ppm): 7.68 (s, 1H, ArH), 7.65-7.63 (m, 2H, ArH), 3.96 (s, 3H, -OCH_3).

Methyl 4-bromo-3-methoxybenzoate 2.0 g (8.2 mmol), copper(I) cyanide 1.5 g (16.4 mmol) copper(I) iodide 1.9 g (9.8 mmol), potassium iodide 1.8 g (10.8 mmol) and 50mL of DMF were stirred at 140°C for 8h under pretection of argon. After the reaction mixture was cooled down to RT, it was filtered, and the filtrate was poured into 150 mL of water, followed by extraction with ethyl acetate (30 mL × 3). The organic layers were combined and washed with water and brine, then dried over anhydrous Na_2SO_4. After the solvent was removed, the crude product was purified by column chromatograph over silica using petroleum ether/dichloromethane (1/1) as eluent to obtaine methyl 4-cyano-3-methoxybenzoate as a white solid. Yield: 60%, m.p.: 112-115°C. ^{1}H NMR (400 MHz, $CDCl_3$) δ(ppm): 7.37 (d, J = 8.4 Hz, 1H, ArH), 7.62 (d, J = 2.8 Hz, 1H, ArH), 7.14 (dd, J = 8.8 Hz, 2.8 Hz, 1H, ArH), 3.92 (s, 3H, -OCH_3).

Methyl 4-cyano-3-methoxybenzoate 3.4 g (18.1 mmol), 50% anhydrous sodium hydroxide (3.0 e.q.) and 30mL of methanol were mixed and stirred at 80°C for 1h. After the reactant was cooled down, it was poured into 150 mL of water, then aqueous hydrochloric acid was added so that the pH value was adjusted to ~1. The white precipitate was collected through filtration, washed with water, and recrystallized from methanol to aford 4-cyano-3-methoxybenzoic acid (**1f**) as white solid. Yield: 86%; m.p.:106-108°C.

Synthesis of 3-cyano-4-methoxybenzoic acid (1g)

3-Cyano-4-methoxybenzoic acid (**1g**) was synthesized with the similar bromation, cyanation and hydrolysis procedures of **1f**, using methyl 4-methoxybenzoate rather than methyl 3-hydroxybenzoate as the reactant. White solid. m.p.:250-251°C.

General synthetic procedure for the cyclometallate ligands 2b~2f.[11]

10 mmol of the carboxylic acid (**1b~1g**) was refluxed with 20 mL thionyl chloride for 1 h, then the excessive thionyl chloride was removed in vacuum. The residue was dissolved in 20 mL dry CH_2Cl_2, then added dropwisely into a mixture of 11 mmol of *N*-phenylbenzene-1, 2-diamine, 2 mL of triethylamine, and 40 mL of dry CH_2Cl_2. After being stirred at room temperature for 24 h, the mixture was poured into 100 mL of water, and extracted with dry CH_2Cl_2 (3 × 20 mL). The organic layers were combined and washed with water and brine, then dried over anhydrous Na_2SO_4. After the solvent was removed and dried for 24 h at 50 °C under a vacuum of 1.5 KPa, the intermediate was refluxed in 30 mL of acetic acid for 12 h, then poured into 100 mL of water followed by extraction with ethyl acetate (4 × 30 mL). The organic layers were combined and washed with water and brine, and then dried over anhydrous Mg_2SO_4. After the solvent was removed, the crude product was purified by column chromatograph over silica using petroleum ether/ethyl acetate (8/1) as eluent to yield the pure product.

2-(3-Methoxyphenyl)-1-phenyl-1*H*-benzo[*d*]imidazole (**2b**). Gray solid. Yield: 82.6%; m.p.: 136-137 °C. ^{1}H NMR (400 MHz, $CDCl_3$) δ(ppm): 7.86 (d, J = 8.0 Hz, 1H, ArH), 7.53-7.45 (m, 5H, ArH), 7.33-7.30 (m, 3H, ArH), 7.22 (t, J = 7.2 Hz, 2H, ArH), 6.82 (d, J = 8.4 Hz, 2H, ArH), 3.80 (s, 3H, -OCH_3).

2-(4-Methoxyphenyl)-1-phenyl-1*H*-benzo[*d*]imidazole (**2c**). White solid. Yield: 71.5%; m.p.: 135-136 °C. ^{1}H NMR (400 MHz, $CDCl_3$) δ(ppm): 7.90 (d, J = 8.0 Hz, 1H, ArH), 7.59-7.49 (m, 5H, ArH), 7.37-7.32 (m, 3H, ArH), 7.22 (t, J = 7.2 Hz, 2H, ArH), 6.90-6.82 (m, 2H, ArH), 3.80 (s, 3H, -OCH_3).

2-(3-Cyanophenyl)-1-phenyl-1*H*-benzo[*d*]imidazole (**2d**). Light cyan solid. Yield: 73.6%; m.p.: 139-140 °C. ^{1}H NMR (400 MHz, $CDCl_3$) δ(ppm): 7.91-7.88 (m, 2H, ArH), 7.80 (d, J = 8.0 Hz, 1H, ArH), 7.6 (d, J = 7.6 Hz, 1H, ArH), 7.58-7.52 (m, 3H, ArH), 7.44-7.36 (m, 2H, ArH), 7.33-7.30 (m, 3H, ArH), 7.27-7.26 (m, 1H, ArH).

2-(4-Cyanophenyl)-1-phenyl-1*H*-benzo[*d*]imidazole (**2e**). Yellow solid. Yield: 67.6%; m.p.: 117-118 °C. ^{1}H NMR (400 MHz, $CDCl_3$) δ(ppm): 7.90 (d, J = 8.0 Hz, 1H, ArH), 7.69 (d, J = 8.4 Hz, 2H, ArH),7.60-7.53 (m, 5H, ArH), 7.38 (t, J = 7.2 Hz, 1H, ArH), 7.34-7.30 (m, 3H, ArH), 7.27-7.26 (m, 1H, ArH).

2-(4-Cyano-3-methoxyphenyl)-1-phenyl-1*H*-benzo[*d*]imidazole (**2f**). White solid. Yield: 63.6%; m.p.: 139-140 °C. ^{1}H NMR (400 MHz, $CDCl_3$) δ(ppm): 7.90 (d, J = 8.0 Hz, 1H, ArH), 7.59-7.51 (m, 3H, ArH), 7.45 (d, J = 8.0 Hz, 1H, ArH), 7.40-7.32 (m, 4 H, ArH), 7.29 (s, 1H, ArH), 7.25-7.24 (m, 1H, ArH), 7.14 (dd, J = 8.0 Hz, 1.6 Hz, 1H, ArH), 3.78 (s, 3H, -OCH_3).

2-(3-Cyano-4-methoxyphenyl)-1-phenyl-1*H*-benzo[*d*]imidazole (**2g**). Light green solid. Yield 77.6%; m.p.: 139-140 °C. ^{1}H NMR (400 MHz, $CDCl_3$) δ(ppm): 7.91-7.88 (m, 2H, ArH), 7.70 (d, J = 9.2 Hz, 1H, ArH), 7.56-7.53 (m, 3H, ArH), 7.38-7.22 (m, 5 H, ArH), 7.14 (t, J = 8.8 Hz, 1H, ArH), 3.95 (s, 3H, -OCH_3).

General synthetic procedures for the objective complexes (**4b~4g**).

The dichloro-bridged iridium(III) complexes (**3b~3g**) were prepared by refluxing $IrCl_3 \cdot nH_2O$ (1 mmol) with cyclometallate ligands **2b~2g** (2.4 mmol) in a mixture of 2-ethoxyethanol and water (3 : 1) under argon for 24 h. The precipitates were filtered and washed with methanol (3 × 15 mL), then dried over vacuum to afford **3b~3g**. The objective compounds **4b~4g** were prepared by refluxing the chloride-bridged dimers **3b~3g** (0.1 mmol), acetylacetone (0.3 mmol) and sodium carbonate (1 mmol) in 10 mL of 2-ethoxyethanol under argon for 12 h. After being cooled down, the precipitates were collected and purified from flash chromatography through silica column using cyclohexane/ethyl acetate = 5:1 as the eluent, followed by more than three times recrystallization procedure to render satisfied purity, then dried for 24 h at 100 °C under a vacuum of 1.5 KPa.

Bis(2-(3-methoxyphenyl)-1-phenyl-1*H*-benzo[*d*]imidazole-*N*,*C*$^{2'}$)iridium(III)(acetylacetonate)

(**4b**:Ir3MOpbi). Yellow solid. Yield: 46.2%; m.p.: > 280 °C. ^{1}H NMR (400 MHz, DMSO-d_6) δ(ppm): 7.88-7.79 (m, 8H, ArH), 7.70-7.68 (m, 2H, ArH), 7.57-7.55 (m, 2H, ArH), 7.39-7.36 (m, 4H, ArH), 7.20-7.18 (m, 2H, ArH), 6.28 (dd, J = 8.4 Hz, 2.4 Hz, 2H, ArH), 6.14 (d, J = 8.4 Hz, 2H, ArH), 6.03 (d, J = 2.8 Hz, 2H, ArH), 5.27 (s, 1H, -CH), 3.28 (s, 6H, -OCH_3), 1.80 (s, 6H, -CH_3). ^{13}C NMR (100 MHz, $CDCl_3$) δ (ppm): 183.8, 164.0, 153.9, 140.6, 136.4, 135.6, 134.8, 130.2, 130.2, 130.0, 128.6, 128.5, 124.0, 122.9, 116.8, 116.6, 110.3, 110.1, 101.4, 54.6, 28.6. ESI-MS: m/z 913.2339 $(M + Na)^+$; Calcd. For $(M_w + Na)^+$: 913.2342.

Bis(2-(4-methoxyphenyl)-1-phenyl-1*H*-benzo[*d*]imidazole-*N*,*C*$^{2'}$)iridium(III)(acetylacetonate)

(**4c**:Ir4MOpbi). Green solid. Yield: 41.5%; m.p.: 266-268 °C. ^{1}H NMR (400 MHz, DMSO-d_6) δ(ppm): 7.83-7.77 (m, 8H, ArH), 7.54-7.52 (m, 4H, ArH), 7.38-7.32 (m, 4H, ArH), 7.12 (d, J = 7.6 Hz, 2H, ArH), 6.37 (d, J = 8.8 Hz, 2H, ArH), 6.15 (dd, J = 8.4 Hz, 2.4 Hz, 2H, ArH), 5.74 (d, J = 2.4 Hz, 2H, ArH), 5.30 (s, 1H, -CH), 3.31 (s, 6H, -OCH_3), 1.80 (s, 6H, -CH_3). ^{13}C NMR (100 MHz, $CDCl_3$) δ(ppm): 184.9, 164.2, 159.6, 151.8, 140.7, 136.5,

135.9, 130.3, 129.8, 128.6, 128.4, 128.3, 126.2, 123.8, 122.5, 119.9, 116.4, 110.1, 106.0, 101.5, 54.4, 28.6. ESI-MS: m/z 913.2348 $(M + Na)^+$; Calcd. For $(M_w + Na)^+$: 913.2342.

Bis(2-(3-cyanophenyl)-1-phenyl-1*H*-benzo[*d*]imidazole-*N*,$C^{2'}$)iridium(III)(acetylacetonate) (**4d**:Ir3CNpbi). Green powder. Yield: 43.6%; m.p.: 253-255 °C. ^{1}H NMR (400 MHz, DMSO-d_6) δ(ppm): 7.87-7.82 (m, 10H, ArH), 7.58-7.56 (m, 2H, ArH), 7.47-7.45 (m, 4H, ArH), 7.29-7.26 (m, 2H, ArH), 6.90 (dd, J = 8.0, 1.2 Hz, 2H, ArH), 6.58-6.56 (m, 4H, ArH), 5.33 (s, 1H, -CH), 1.84 (s, 6H, $-CH_3$). ^{13}C NMR (100 MHz, $CDCl_3$) δ(ppm): 185.5, 161.7, 159.0, 139.8, 136.4, 135.6, 134.6, 131.4, 130.9, 130.9, 130.8, 128.1, 127.9, 127.4, 124.8, 124.2, 116.6, 111.1, 103.2, 101.7, 28.4. ESI-MS: m/z 903.2034 $(M + Na)^+$; Calcd. For $(M_w + Na)^+$: 903.2035.

Bis(2-(4-cyanophenyl)-1-phenyl-1*H*-benzo[*d*]imidazole-*N*,$C^{2'}$)iridium(III)(acetylacetonate) (**4e**:Ir4CNpbi). Orange crystal. Yield: 40.8%; m.p.: > 280 °C. ^{1}H NMR (400 MHz, DMSO-d_6) δ(ppm): 7.89-7.77 (m, 10H, ArH), 7.60-7.57 (m, 2H, ArH), 7.50-7.44 (m, 4H, ArH), 7.27-7.25 (m, 2H, ArH), 7.02 (dd, J = 8.4, 1.6 Hz, 2H, ArH), 6.68 (d, J = 1.2 Hz, 2H, ArH), 6.59 (d, J = 8.4 Hz, 2H, ArH), 5.29 (s, 1H, -CH), 1.81 (s, 6H, $-CH_3$). ^{13}C NMR (100 MHz, $CDCl_3$) δ(ppm): 185.4, 161.8, 148.4, 137.7, 134.9, 130.7, 130.6, 128.2, 128.2, 124.9, 124.4, 124.4, 124.2, 116.6, 111.3, 111.2, 101.7, 28.4. ESI-MS: m/z 903.2036 $(M + Na)^+$; Calcd. For $(M_w + Na)^+$: 903.2035.

Bis(2-(4-cyano-3-methoxyphenyl)-1-phenyl-1*H*-benzo[*d*]imidazole-*N*,$C^{2'}$)iridium(III) (acetylacetonate) (**4f**:Ir3MO4CNpbi). Red solid. Yield: 46.5%; m.p.: 245-246 °C. ^{1}H NMR (400 MHz, DMSO-d_6) δ(ppm): 7.92 (d, J = 7.6 Hz, 2H, ArH), 7.88-7.82 (m, 8H, ArH), 7.58-7.56 (m, 2H, ArH), 7.48-7.45 (m, 4H, ArH), 7.31-7.30 (m, 2H, ArH), 6.49 (s, 2H, ArH), 6.23 (s, 2H, ArH), 5.27 (s, 1H, CH), 3.28 (s, 6H, $-OCH_3$), 1.80 (s, 6H, $-CH_3$). ^{13}C NMR (100 MHz, $CDCl_3$) δ(ppm): 185.3, 161.8, 156.2, 140.5, 140.0, 138.0, 136.4, 135.0, 130.6, 130.5, 130.4, 128.6, 128.6, 124.9, 124.5, 117.4, 116.7, 111.1, 107.8, 101.69, 54.9, 28.5. ESI-MS: m/z 963.2244 $(M + Na)^+$; Calcd. For $(M_w + Na)^+$: 963.2247.

Bis(2-(3-cyano-4-methoxyphenyl)-1-phenyl-1*H*-benzo[*d*]imidazole-*N*,$C^{2'}$)iridium(III) (acetylacetonate) (**4g**: Ir3CN4MOpbi). Greenish blue powder. Yield: 40.2%; m.p.: 267-268 °C. ^{1}H NMR (400 MHz, DMSO-d_6) δ(ppm): 7.88 (d, J = 4.0 Hz, 4H, ArH), 7.84-7.80 (m, 4H, ArH), 7.64 (d, J = 7.6 Hz, 2H, ArH), 7.58 (d, J = 7.6 Hz, 2H, ArH), 7.48-7.40 (m, 4H, ArH), 7.23 (d, J = 7.6 Hz, 2H, ArH), 6.47 (s, 2H, ArH), 5.95 (s, 2H, ArH), 5.38 (s, 1H, -CH), 3.21 (s, 6H, -OCH_3), 1.87 (s, 6H, -CH_3). ^{13}C NMR (100 MHz, $CDCl_3$) δ(ppm): 185.5, 162.1, 161.9, 160.3, 139.7, 136.2, 134.6, 130.9, 130.8, 129.0, 128.6, 128.4, 128.1, 127.6, 124.6, 123.8, 118.0, 116.7, 116.3, 110.7, 101.8, 93.6, 54.9, 28.4. ESI-MS: m/z 963.2248 $(M + Na)^+$; Calcd. For $(M_w + Na)^+$: 963.2247.

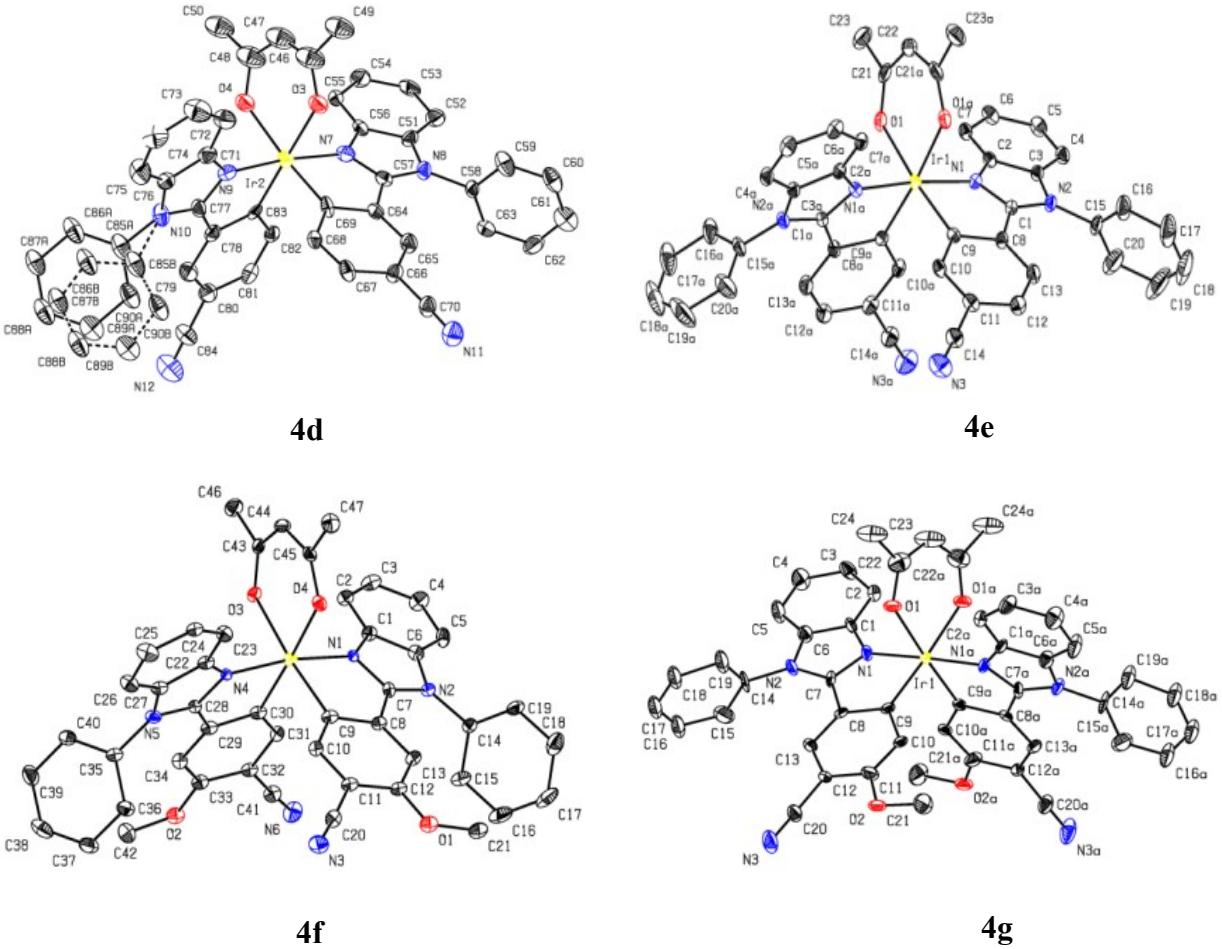

4d **4e**

4f **4g**

Figure S1. **ORTEP** drawing and crystal diagrams of complexes **4d–4g**.

Table S1. Crystal data and structure refinement for complexes **4d–4g**.

Compound	**4d**	**4e**	**4f**	**4g**
Empirical formula	$C_{45}H_{31}IrN_6O_2$	$C_{45}H_{31}IrN_6O_2$	$C_{47}H_{35}IrN_6O_4$	$C_{47}H_{35}IrN_6O_4$
Formula weight	879.96	879.96	940.01	940.01
Temperature	143.00 (10) K	140.00 (10) K	143.00 (10) K	143.00 (2) K
Crystal system	Triclinic	Monoclinic	Triclinic	Tetragonal
Space group	*P*–1	*C*2/*c*	*P*–1	$P4_12_12$
a	13.2009 (4) Å	24.588 (2) Å	12.9834 (6) Å	13.1742 (3) Å
b	15.9948 (4) Å	14.8019 (5) Å	12.9966 (6) Å	13.1742 (3) Å
c	19.2170 (7) Å	18.5369 (15) Å	17.3152 (7) Å	28.3375 (8) Å
α	90.118 (3) deg	90.00 deg	107.588 (4) deg	90.00 deg
β	97.538(3) deg	137.444 (16) deg	97.441(3) deg	90.00 deg
γ	95.431 (2) deg	90.00 deg	110.780 (4) deg	90.00 deg
Volume	4004.1 (2) $Å^3$	4562.8 (11) $Å^3$	2510.5 (2) $Å^3$	4918.3 (2) $Å^3$
Z	4	4	2	4
Calculated density	1.460 mg·mm^{-3}	1.281 mg·mm^{-3}	1.244 mg·mm^{-3}	1.269 mg·mm^{-3}
Absorption coefficient	3.379 mm^{-1}	2.965 mm^{-1}	2.701 mm^{-1}	2.758 mm^{-1}
F(000)	1744.0	1744.0	936.0	1872.0
Crystal size	0.30 × 0.25 × 0.20 mm	0.30 × 0.25 × 0.20 mm	0.30 × 0.20 × 0.20 mm	0.30 × 0.20 × 0.20 mm
Reflections collected	38944	10355	22497	20399
Independent reflections	16322 [*R*(int) = 0.0655]	4660 [*R*(int) = 0.0399]	10246 [*R*(int) = 0.0478]	5010 [*R*(int) = 0.0599]
θ–range for data collection	2.811 to 26.371°	2.892 to 26.371°	2.988 to 26.371°	3.18 to 26.37°
Goodness–of–fit on F^2	0.962	1.068	1.074	1.097
Final *R* indices [$I > 2\sigma(I)$]	R_1 = 0.0633, wR_2 = 0.1242	R_1 = 0.0303, wR_2= 0.0695	R_1 = 0.1010, wR_2 = 0.2737	R_1 = 0.0597, wR_2 = 0.1363
R indices (all data)	R_1 = 0.1133, wR_2 = 0.1431	R_1 = 0.0355, wR_2 = 0.0714	R_1 = 0.1081, wR_2 = 0.2790	R_1 = 0.0640, wR_2= 0.1385
Largest diff. peak and hole	1.91 and –1.15 e·$Å^{-3}$	1.12 and –0.88 e·$Å^{-3}$	15.35 and –3.13 e·$Å^{-3}$	1.59 and –2.90 e·$Å^{-3}$

Table S2. Optimized Geometry Parameters of the objective complexes **4a–4g** by B3LYP method.

bond length/Å	**4a**	**4b**	**4c**	**4d**	**4e**	**4f**	**4g**
Ir–O1	2.204	2.206	2.202	2.190(2.150)	2.189(2.145)	2.194(2.147)	2.190(2.133)
Ir–O2	2.204	2.206	2.202	2.190(2.155)	2.189(2.145)	2.194(2.144)	2.190(2.133)
Ir–N1	2.068	2.070	2.070	2.068(2.039)	2.068(2.040)	2.067(1.997)	2.069(2.054)
Ir–N2	2.068	2.070	2.070	2.068(2.050)	2.068(2.040)	2.069(2.047)	2.069(2.054)
Ir–C9	2.013	2.016	2.013	2.007(1.999)	2.013(1.990)	2.016(2.008)	2.008(1.959)
Ir–C22	2.013	2.016	2.014	2.007(1.964)	2.013(1.990)	2.016(2.007)	2.008(1.959)
bond angle/deg							
O1–Ir–O2	86.3	86.2	86.5	86.7 (88.5)	86.9 (87.9)	87.0 (88.6)	86.8 (88.6)
N1–Ir–N2	175.2	174.3	175.0	175.2(172.0)	175.1(174.9)	174.2(171.6)	175.3(178.0)
C13–Ir–C43	92.8	92.7	93.0	93.3 (89.7)	93.0 (92.5)	93.0 (91.0)	93.4 (90.8)
N2–Ir–C13	97.1	96.7	96.9	97.0 (95.1)	97.1 (96.7)	96.8 (94.9)	97.0 (98.9)
N1–Ir–C13	79.5	79.3	79.6	79.7 (80.6)	79.4 (79.8)	79.3 (79.1)	79.8 (79.7)

The data in parentheses are derived from crystal data.

Table 3. Calculated absorption and emission wavelength (nm), major contribution and transition characters for **4a-4g** in CH_2Cl_2 media using B3LYP method, along with the experimental data.

Compd.	$\lambda_{abs\ max}$ [a] (nm)	configuration	nature	$\lambda_{abs\ max}$ [b] (nm)	configuration	nature	$\lambda_{em\ max}$ [c] (nm)	configuration	nature
4a	300 (300)	H-4→L+1 (82%)	π→π*/ LLCT / MLCT	412 (412)	H→L (97%)	MLCT/π→π*	498 (520)	H→L (68%)	MLCT/π→π*
4b	290 (304)	H–5→L (60%) H→L+7 (17%)	π→π*/ MLCT	448 (430)	H→L (98%)	MLCT/π→π*	556 (555)	H→L (82%)	MLCT/π→π*
4c	307 (304)	H–4→L (79%)	MLCT /π→π*	394 (409)	H→L (95%)	MLCT/π→π*	493 (507)	H→L (56%) H–1→L+1 (23%)	MLCT/π→π*
4d	294 (304)	H–5→L (77%)	π→π*/ MLCT	397 (405)	H→L (96%)	MLCT/π→π*	491 (514)	H→L (55%) H–3→L+1 (14%)	MLCT/π→π*
4e	312 (314)	H–5→L (87%)	π→π*/ MLCT	444 (430)	H→L (98%)	MLCT/π→π*	554 (560)	H→L (76%)	MLCT/π→π*
4f	314 (320)	H–5→L (86%)	π→π*/ MLCT	486 (458)	H→L (98%)	MLCT/π→π*	621 (605)	H→L (85%)	MLCT/π→π*
4g	294 (303)	H–4→L (54%) H–3→L+2 (19%)	MLCT /π→π*	377 (392)	H→L (92%)	MLCT/π→π*	477 (496)	H→L (42%) H–1→L+1 (23%)	MLCT/π→π*

[a] $\lambda_{abs\ max}$:The absorption maximum of the more intensive band; [b] $\lambda_{abs\ max}$: the absorption maximum of the weaker band; [c] $\lambda_{em\ max}$: The PL emission maximum (for the calculated $S_0 \rightarrow T_1$ transition energy, a scaling factor[12] of 0.925 is applied).The corresponding experimental data are shown in the parentheses.

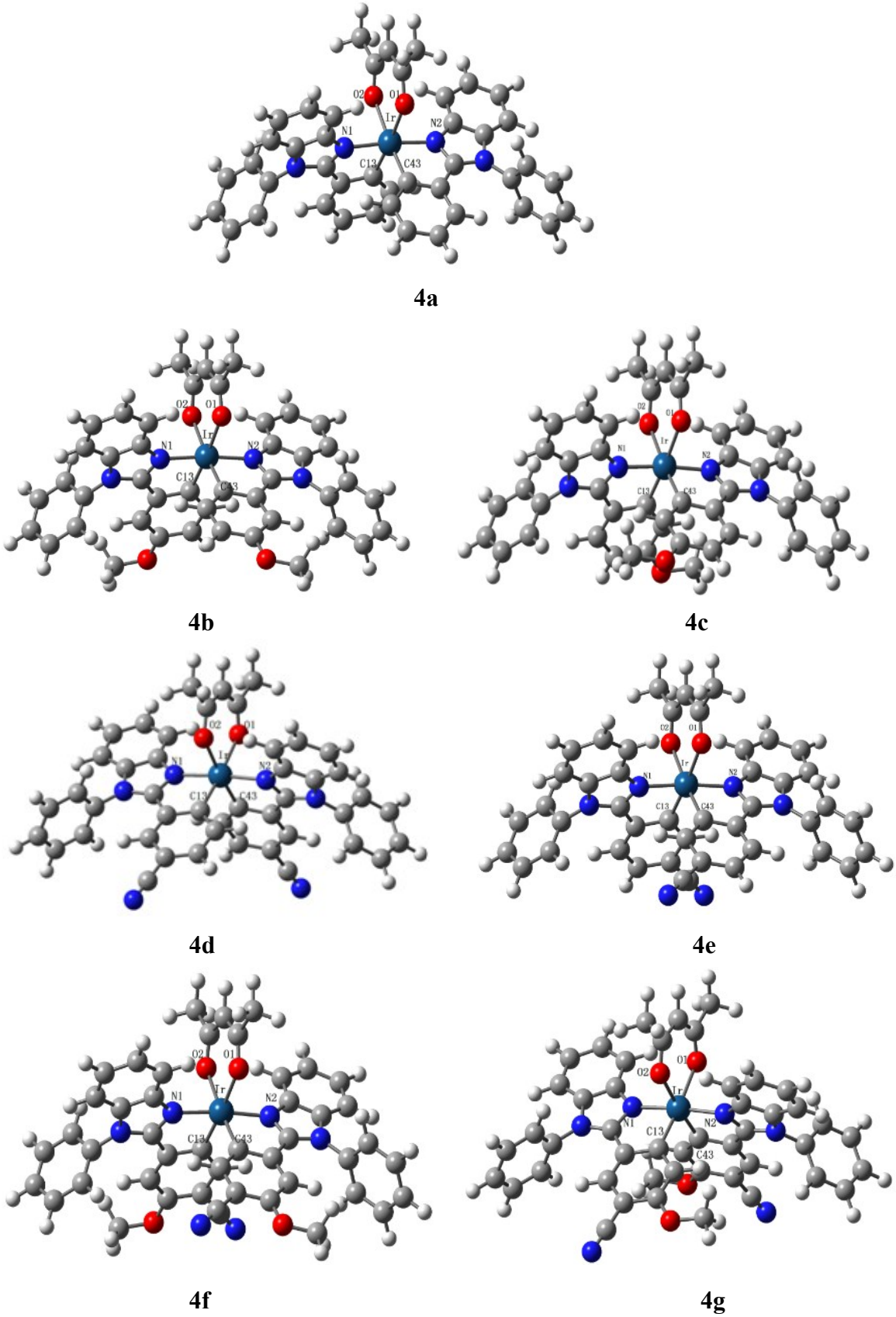

Figure S2. Optimized structures and the numbering of important atoms of **4a–4g**, calculation is conducted at the level of B3LYP/LANL2DZ/6–31(d).

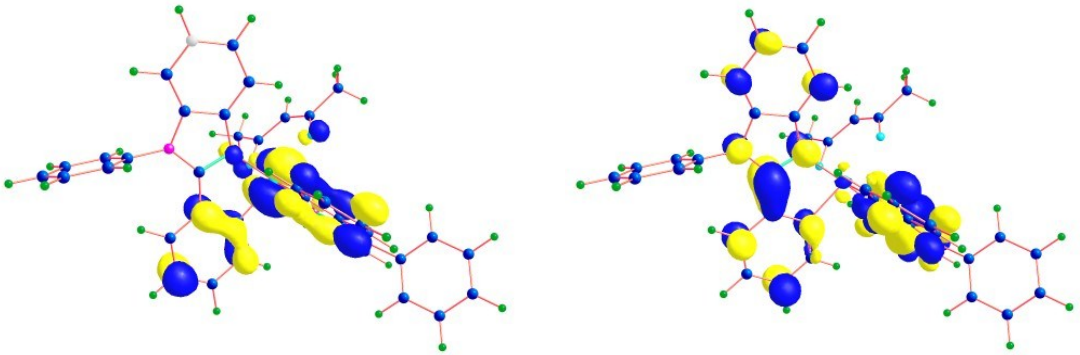

HOMO LUMO

Figure S3. Contour plots of the HOMO and LUMO distribution of parent compound **4a**.

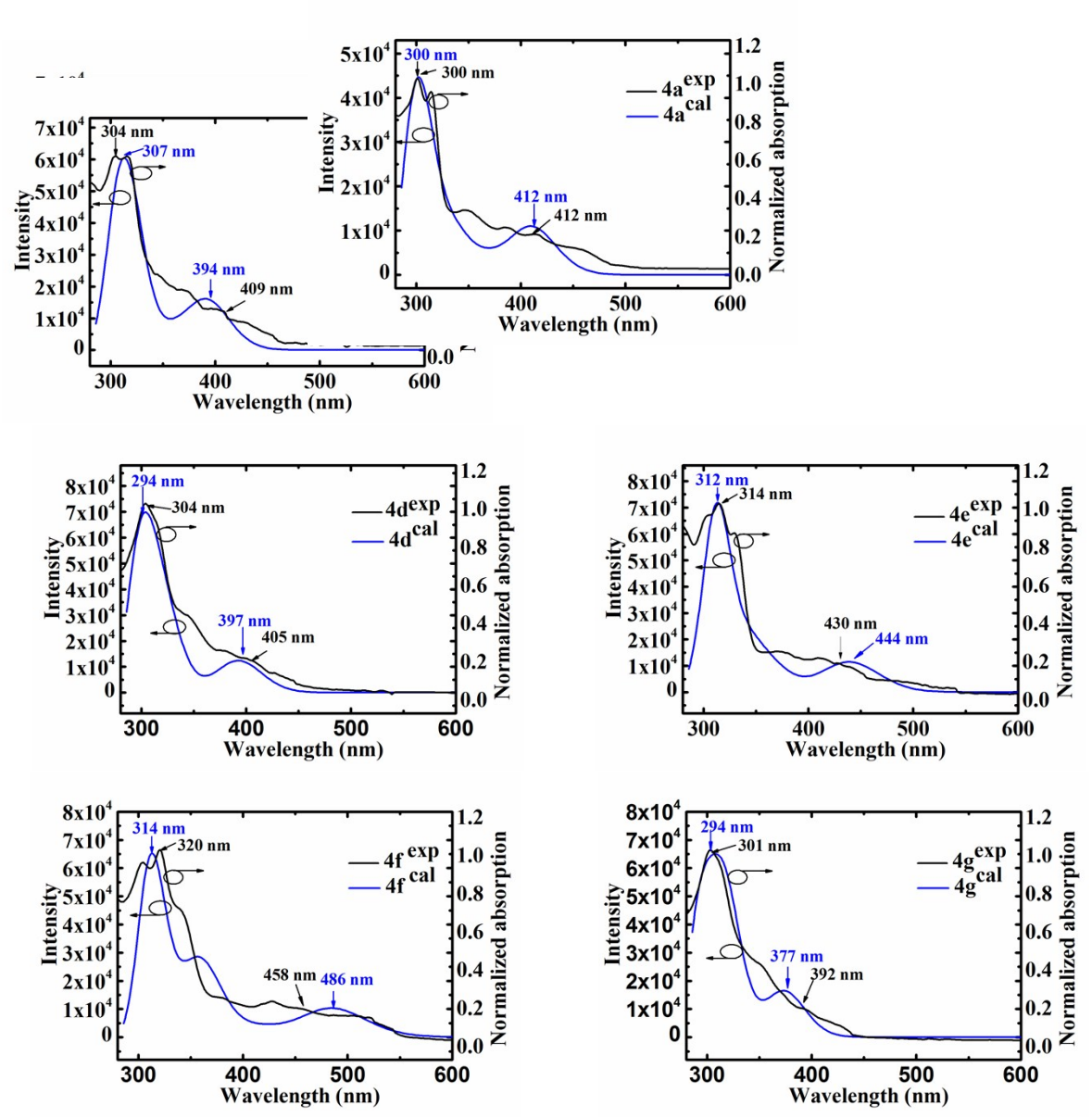

Figure S4. Comparison between experimental UV–Vis absorption spectra (black line) and simulated absorption spectrum (blue line) of **4a–4g** in CH_2Cl_2 media. The absorption maxima of the more intensive band and the relatively weaker band have been identified.

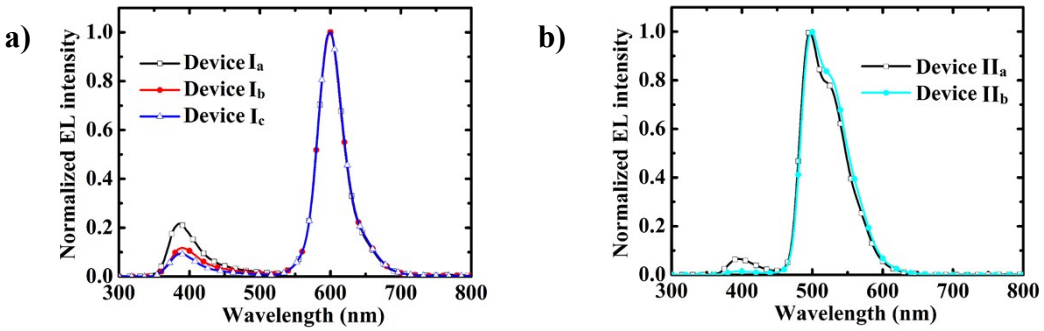

Figure S5. EL spectra of a) Devices $\mathbf{I_a}$~$\mathbf{I_c}$ and b) $\mathbf{II_a}$~$\mathbf{II_b}$.

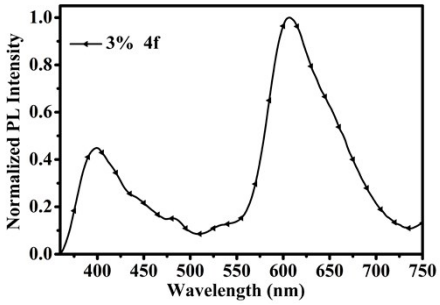

Figure S6. PL spectrum of the 3 wt% **4f**-doped film sample with TCTA as the host.

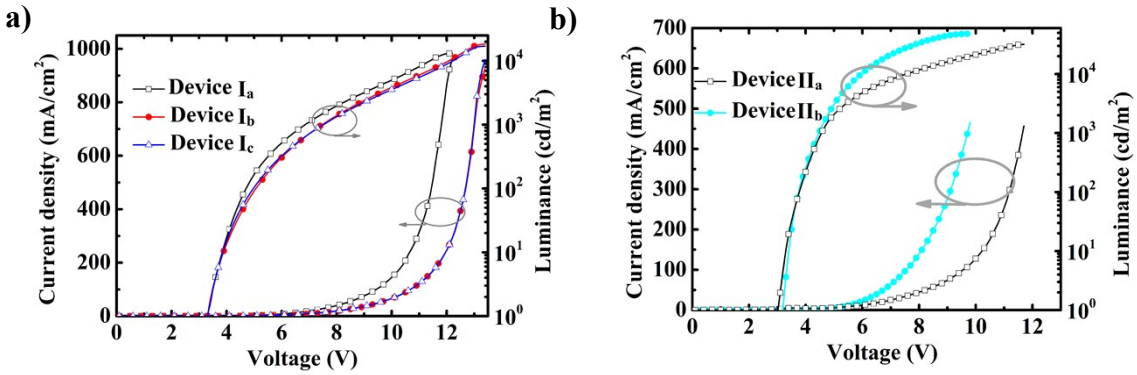

Figure S7. Current density–voltage–luminance (*J–V–L*) characteristics of a) Devices $\mathbf{I_a}$~$\mathbf{I_c}$ and b) $\mathbf{II_a}$~$\mathbf{II_b}$.

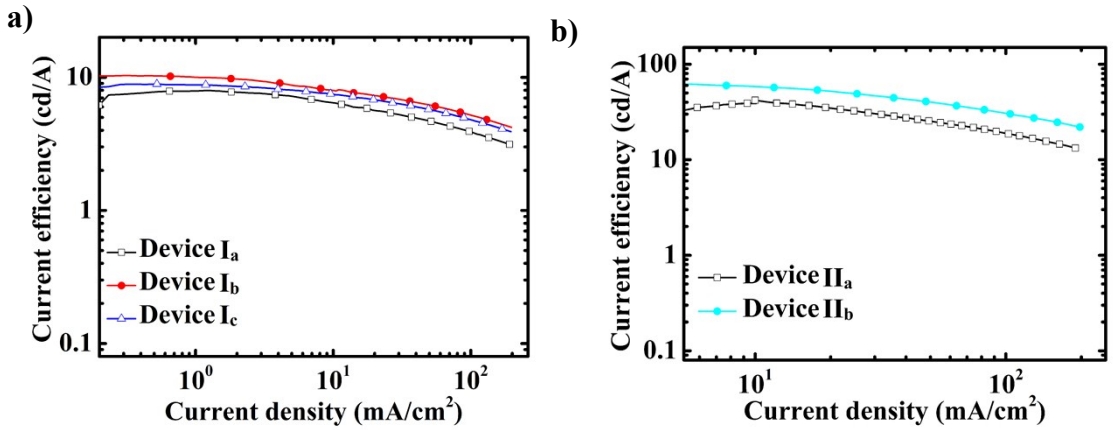

Figure S8. Current efficiency-current density characteristics of a) Devices $\mathbf{I_a}$~$\mathbf{I_c}$ and b) $\mathbf{II_a}$~$\mathbf{II_b}$.

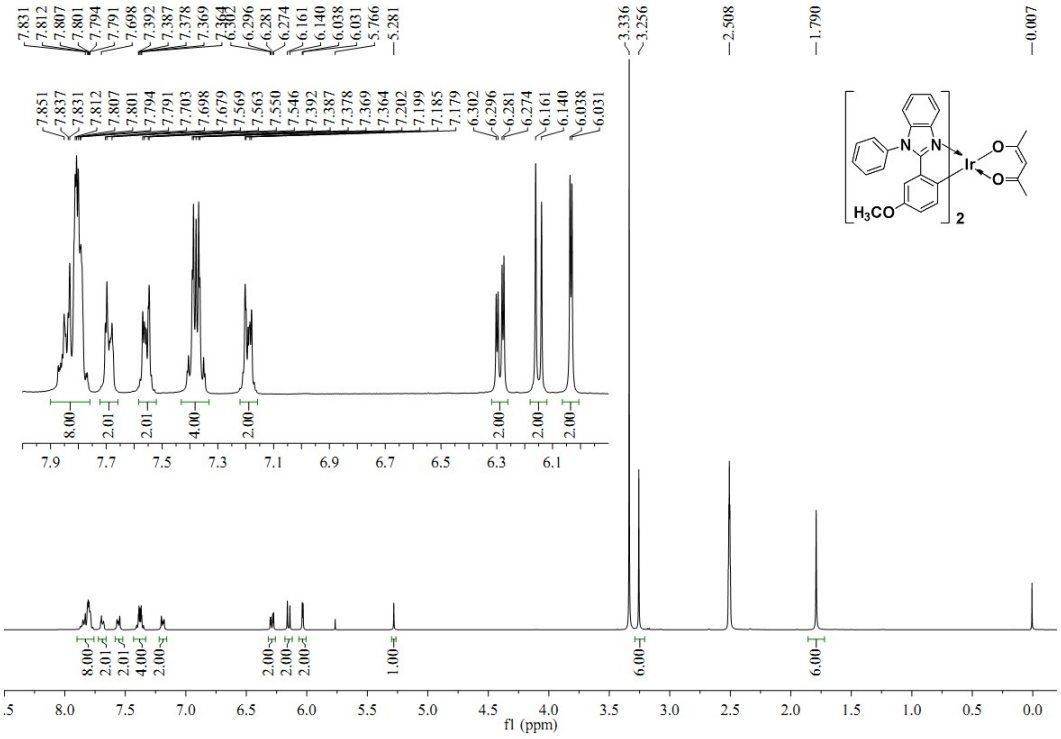

Figure S9. ^{1}H NMR Spectrum of **4b**.

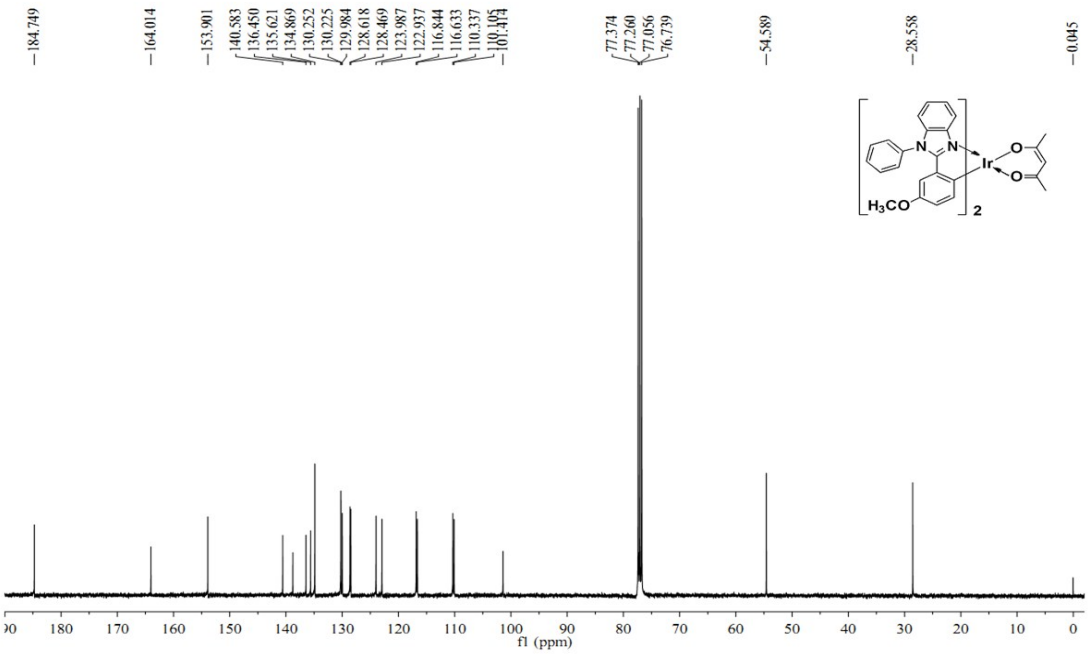

Figure S10. ^{13}C NMR Spectrum of **4b**.

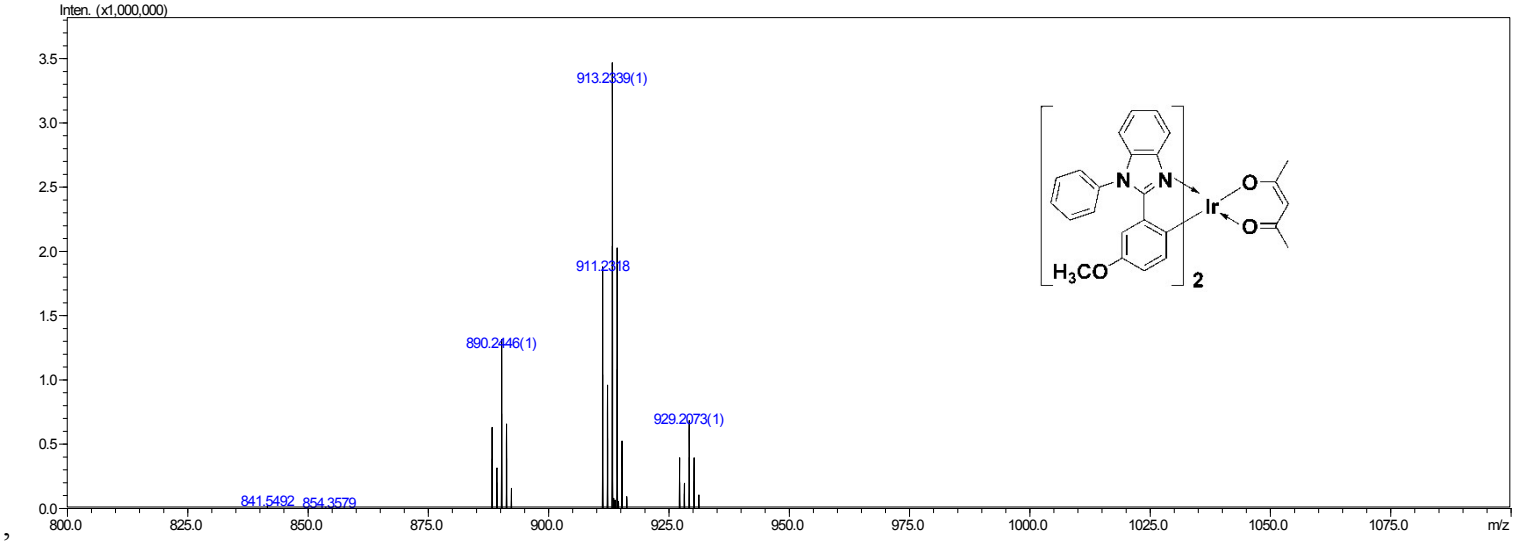

Figure S11. HRMS Spectrum of **4b**.

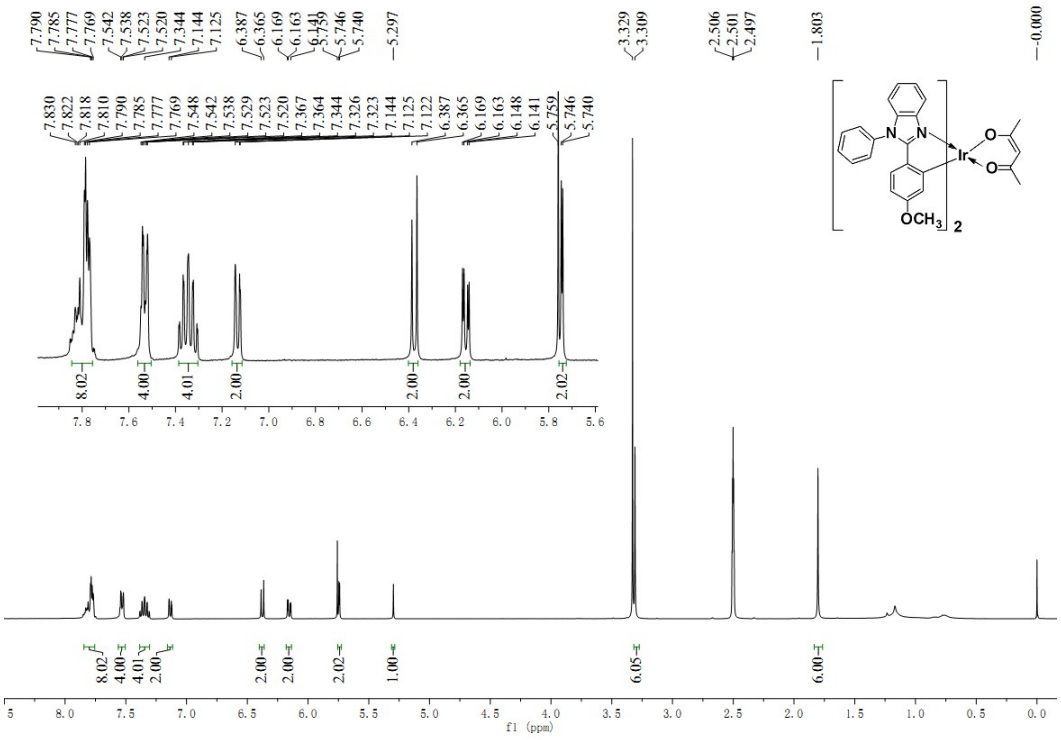

F

igure S12. ^{1}H NMR Spectrum of **4c**.

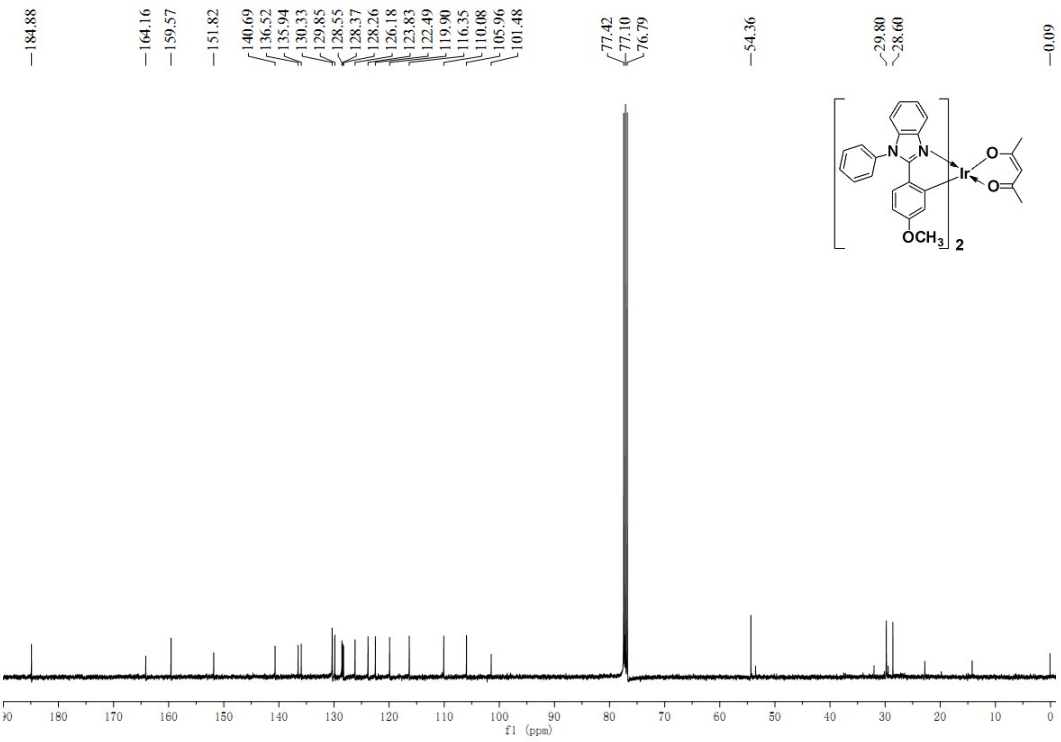

Figure S13. ^{13}C NMR Spectrum of **4c**.

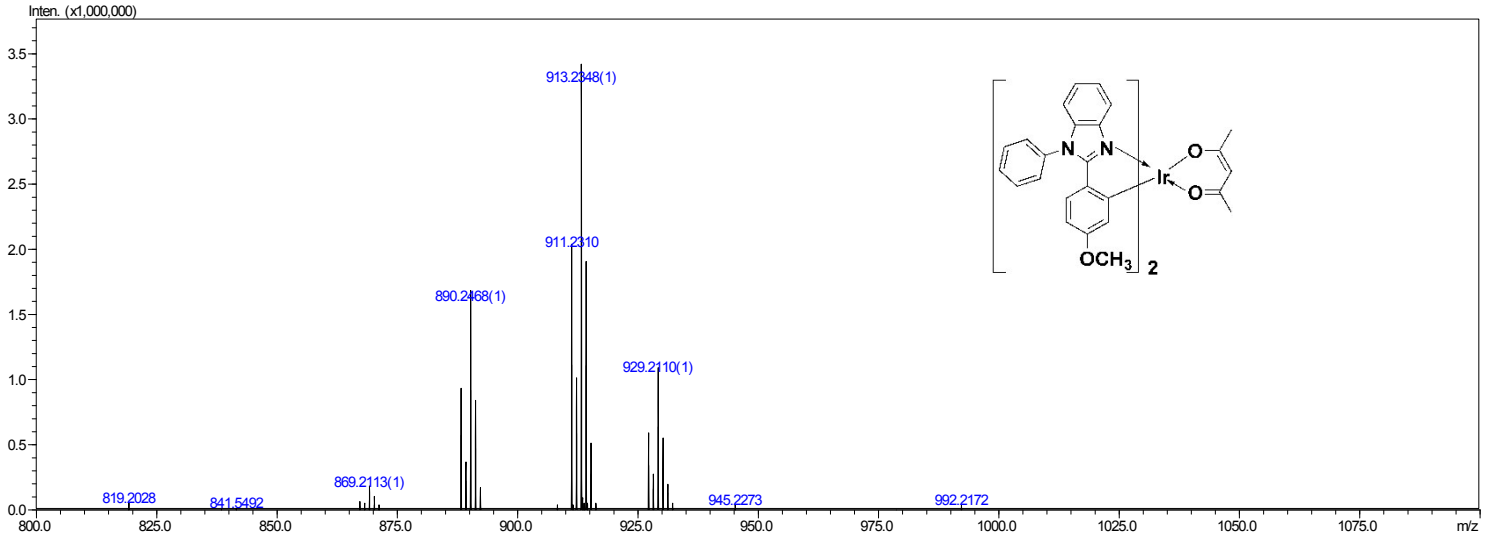

Figure S14. HRMS Spectrum of **4c**.

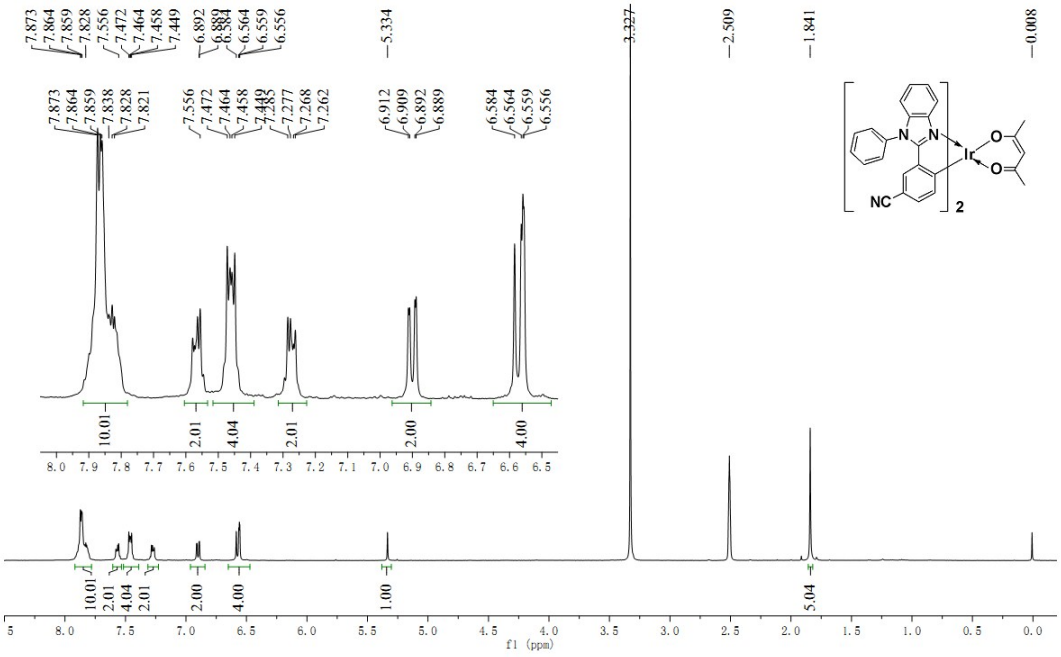

Figure S15. [1]H NMR Spectrum of **4d**.

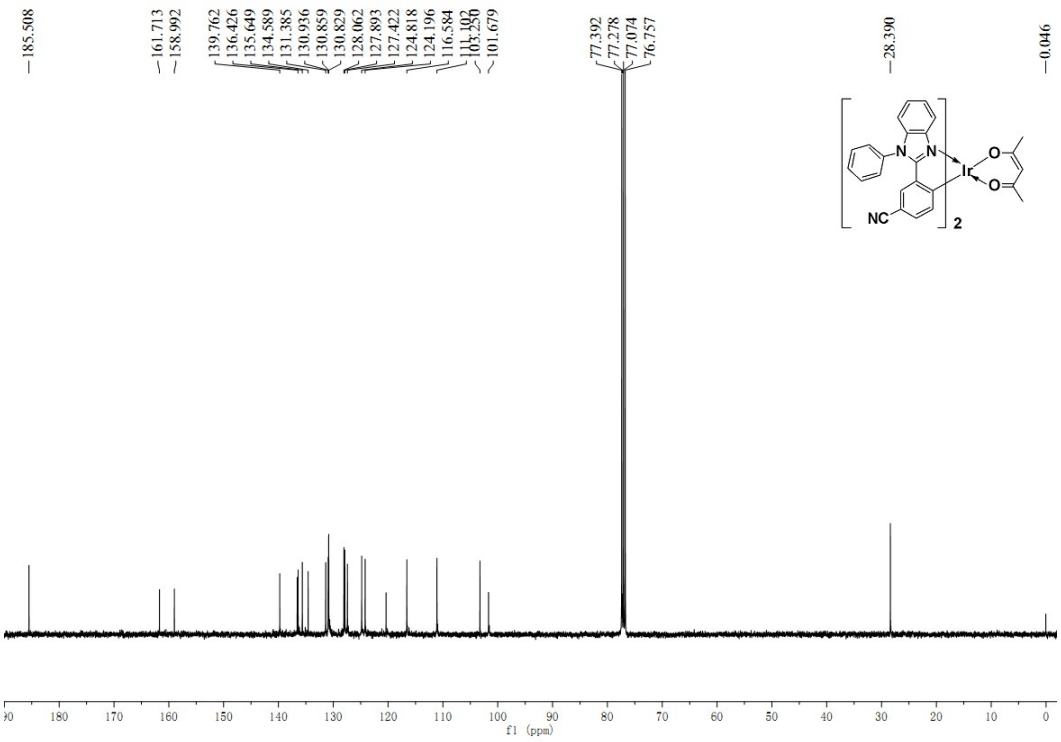

Figure S16. [13]C NMR Spectrum of **4d**.

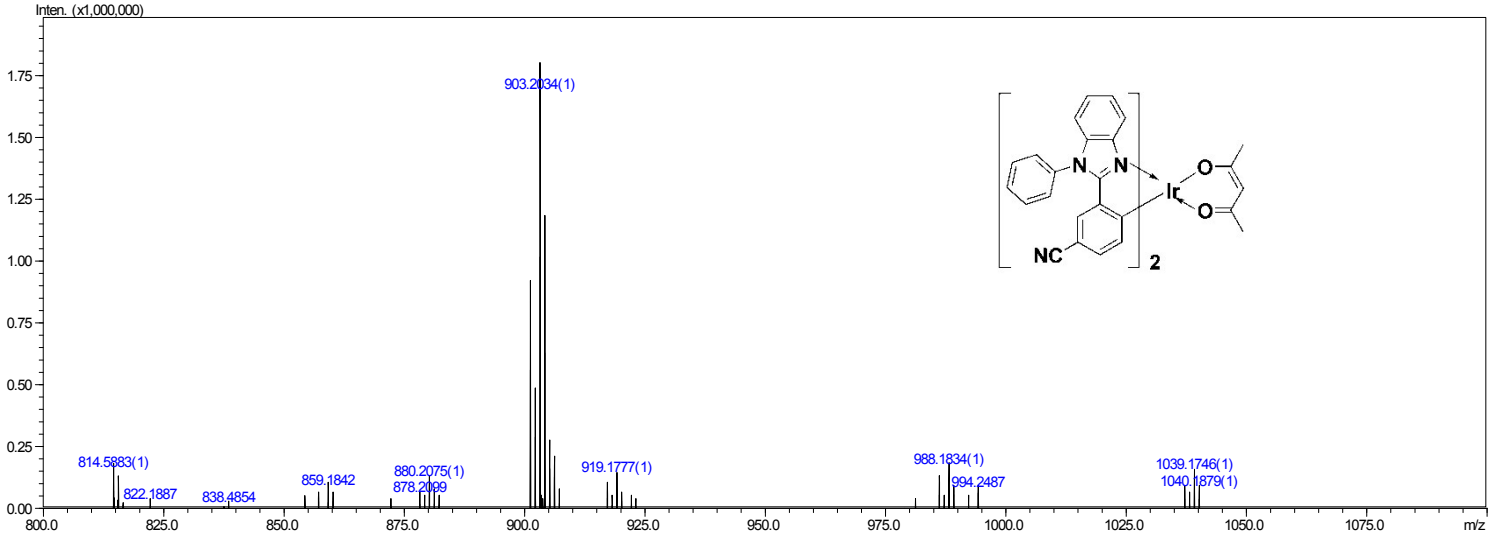

Figure S17. HRMS Spectrum of **4d**.

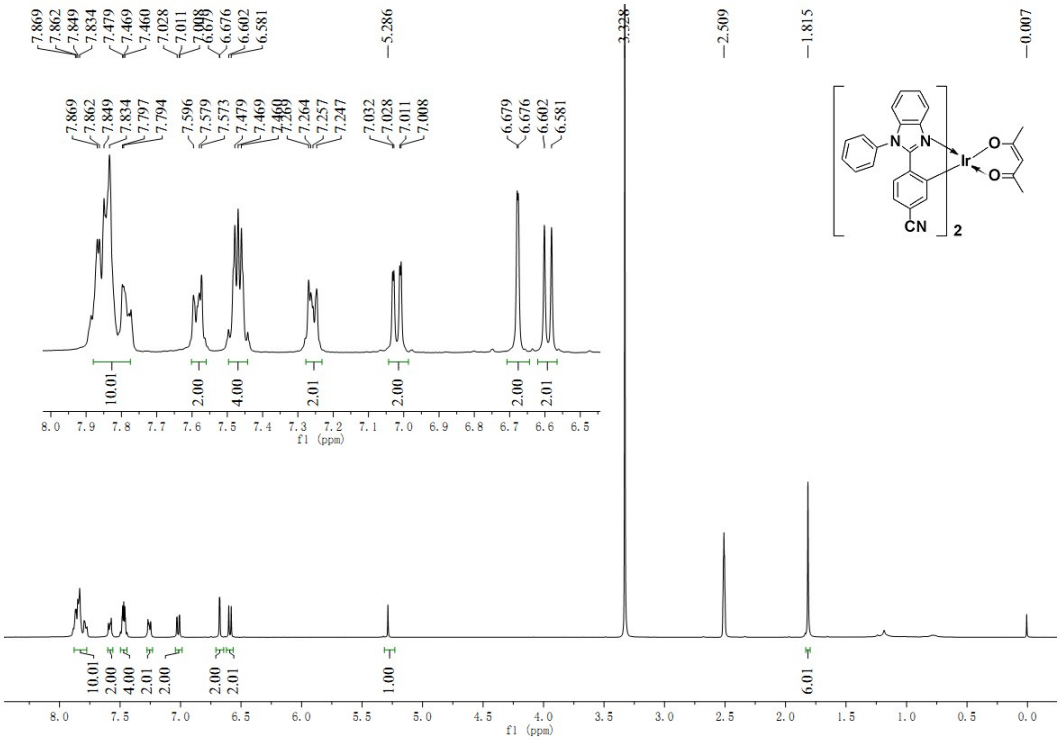

Figure S18. ^{1}H NMR Spectrum of **4e**.

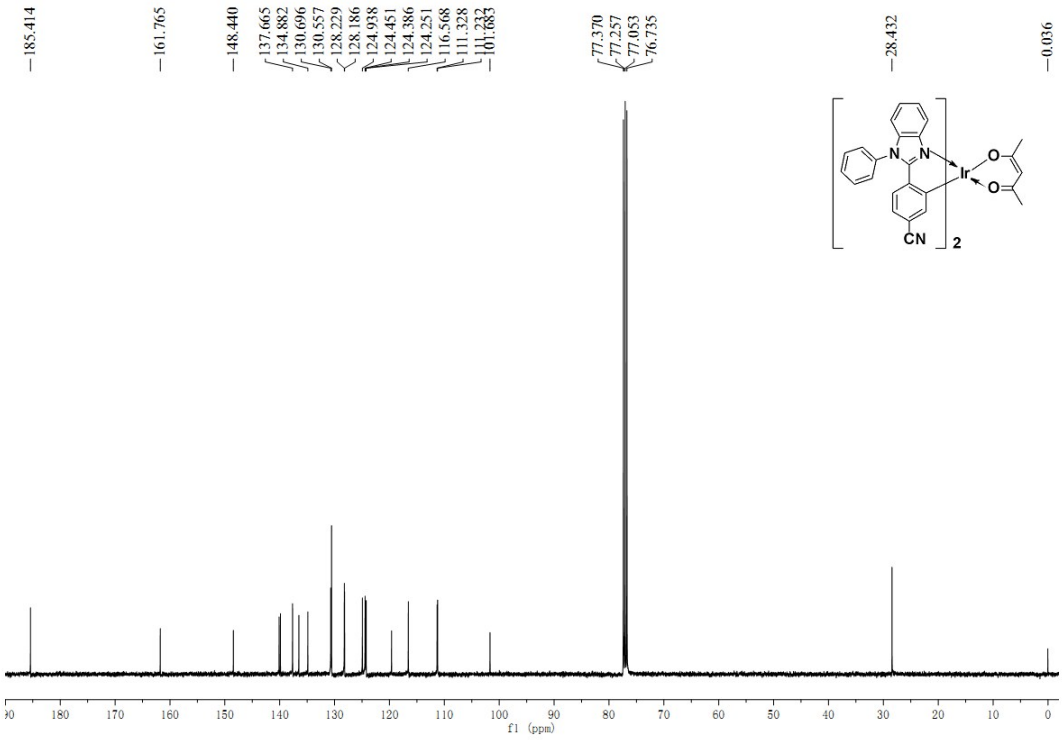

Figure S19. ^{13}C NMR Spectrum of **4e**.

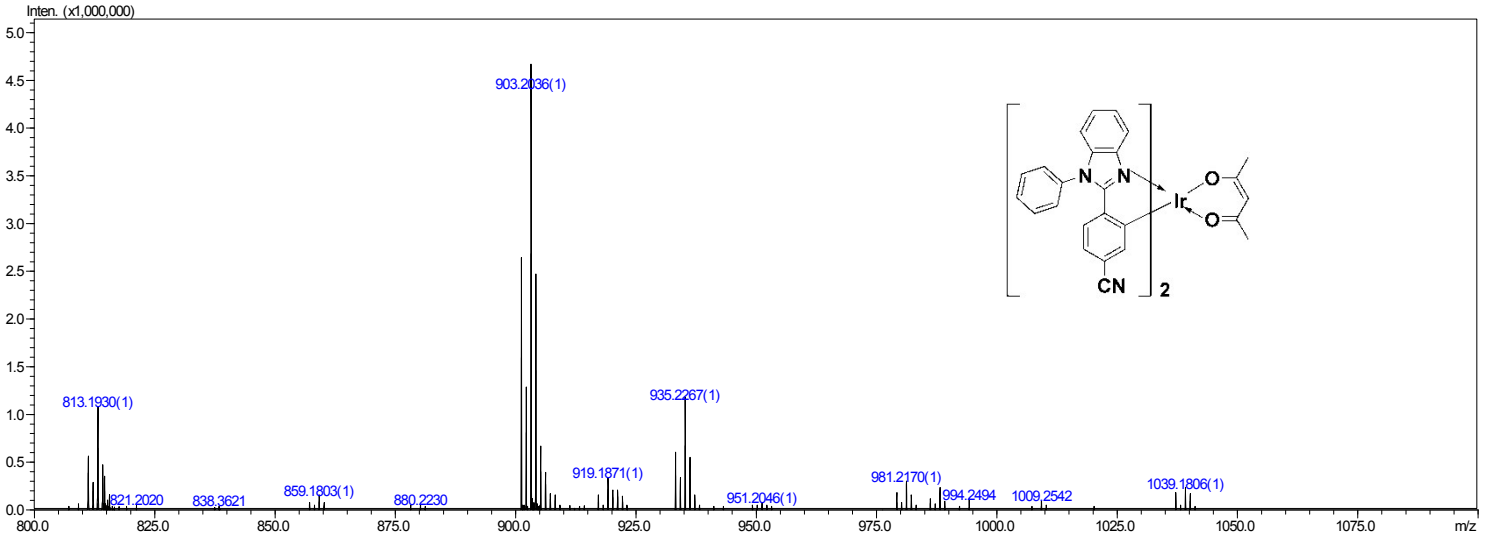

Figure S20. HRMS Spectrum of **4e**.

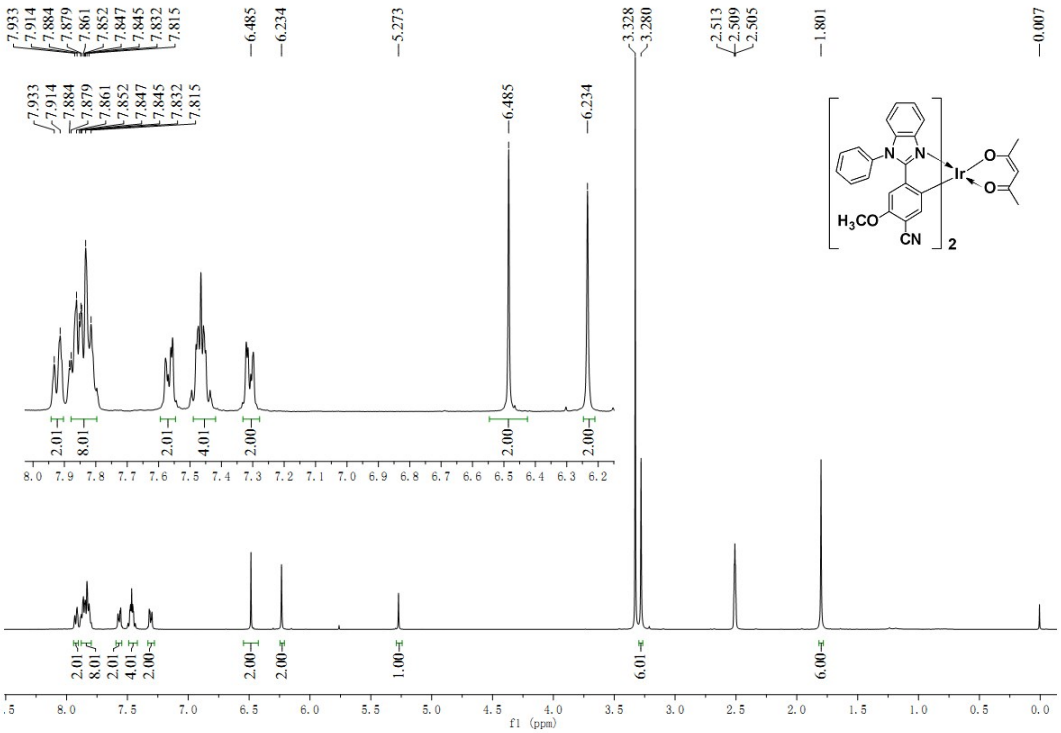

Figure S21. ^{1}H NMR Spectrum of **4f**.

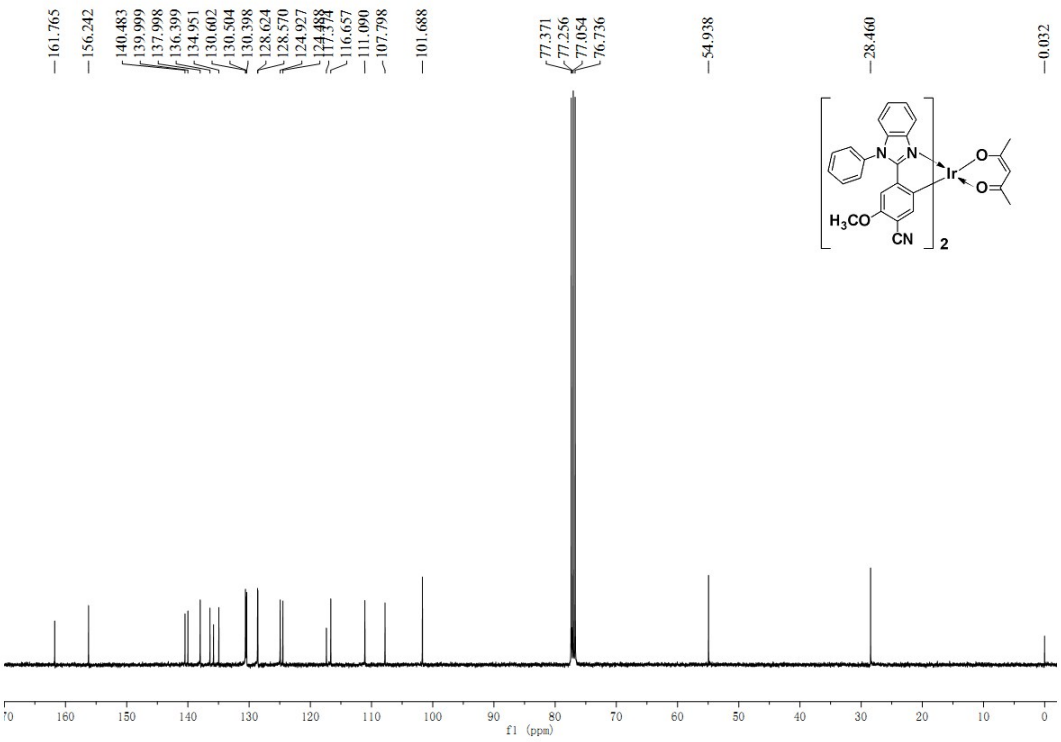

Figure S22. ^{13}C NMR Spectrum of **4f**.

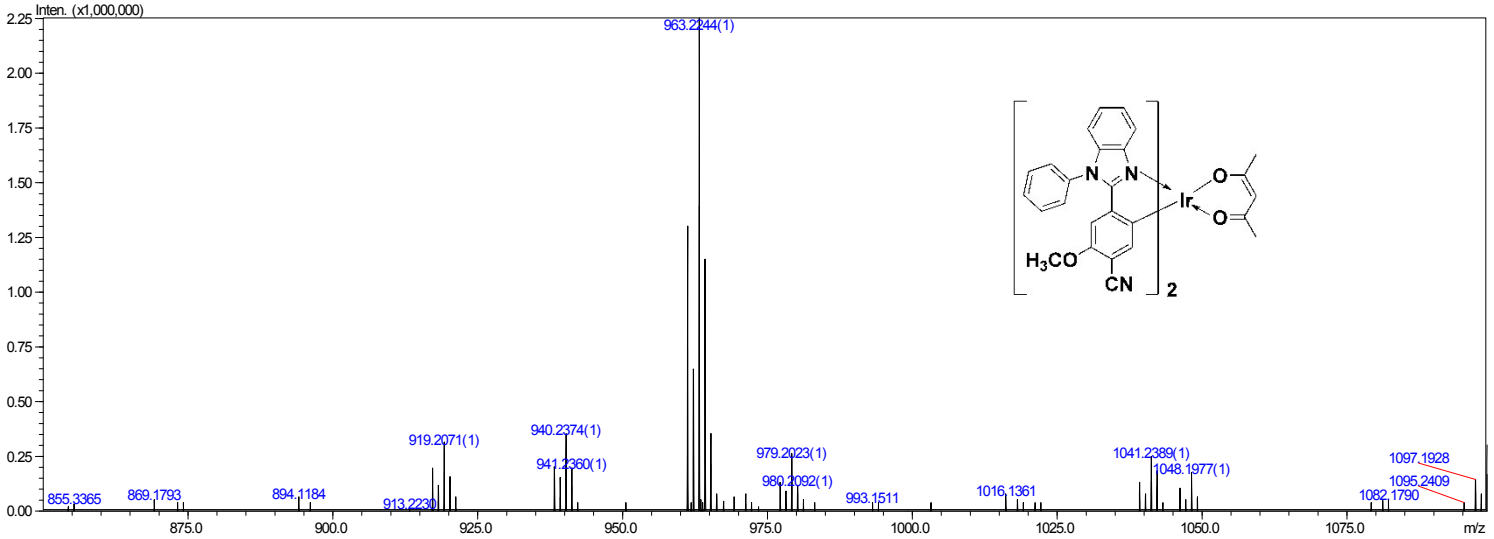

Figure S23. HRMS Spectrum of **4f**.

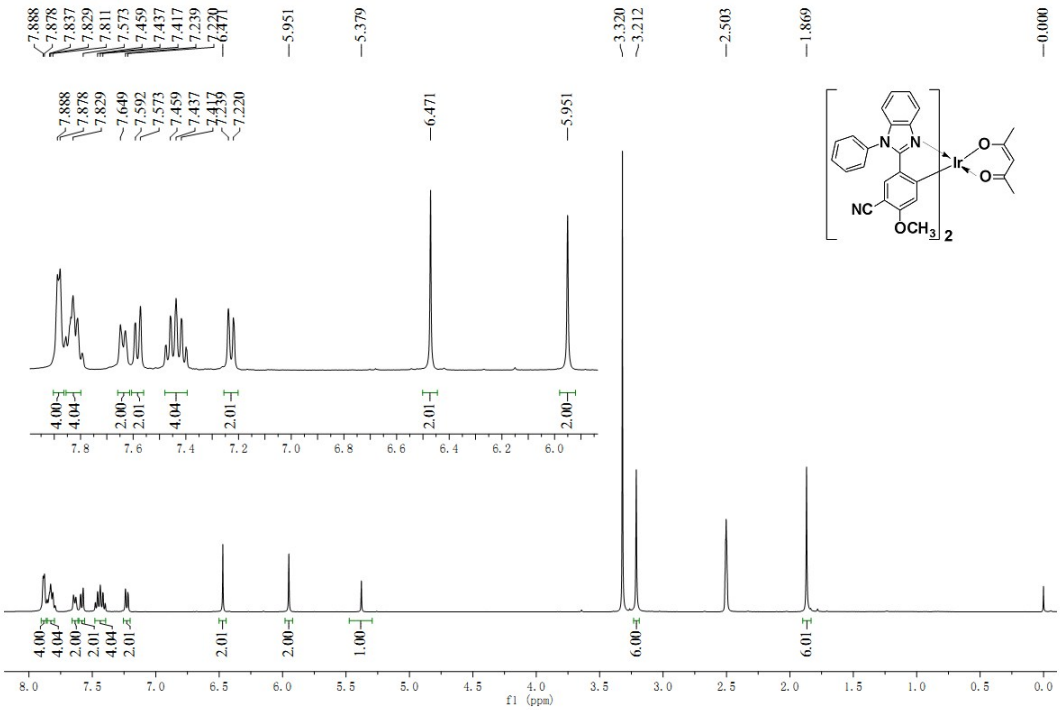

Figure S24. ^{1}H NMR Spectrum of **4g**.

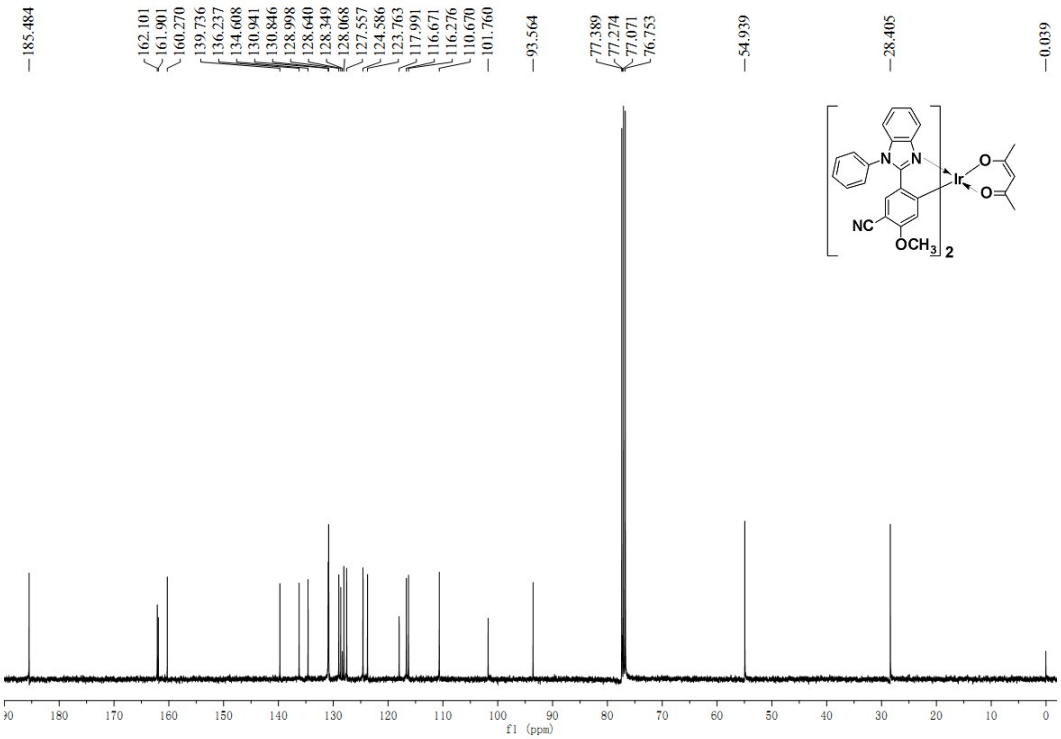

Figure S25. ^{13}C NMR Spectrum of **4g**.

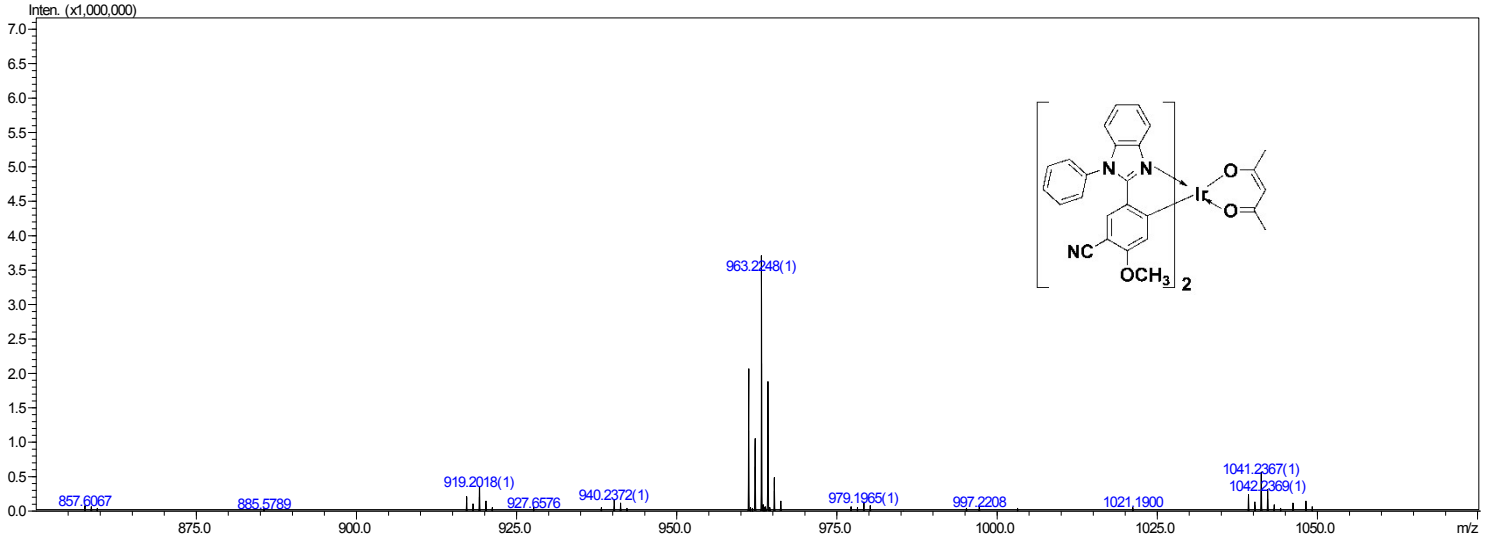

Figure S26. HRMS Spectrum of **4g**.

Table S4. Frontier molecular orbital energies (eV) and compositions (%) of different fragments for complex **4a** in the ground state, derived from DFT/B3LYP calculations in CH_2C1_2 media.

		Contribution (%)					
MO	Energy (eV)	Ir–d	bi[a)]	phen–1[b)]	phen–2[c)]	acac	assignment
LUMO+3	–0.61	0.5	9.6	1.9	87.1	1.0	π*(C^N)
LUMO+2	–0.77	2.2	5.7	3.9	1.0	87.0	π*(acac)
LUMO+1	–1.26	3.0	59.1	33.8	1.9	2.3	π*(C^N)
LUMO	–1.29	2.4	58.4	36.6	1.5	1.2	π*(C^N)
HOMO	–5.03	52.3	10.0	32.5	0.1	5.0	d(Ir) + π(C^N)
HOMO–1	–5.33	47.8	17.4	6.4	0.6	27.9	d(Ir) + π(acac) + π(C^N)
HOMO–2	–5.67	53.6	28.9	11.8	1.0	4.8	d(Ir) + π(C^N)
HOMO–3	–5.77	0.5	42.9	27.0	0	29.3	π(C^N) + π(acac)
HOMO–4	–6.11	12.8	37.2	18.7	2.7	28.5	d(Ir) + π(acac) + π(C^N)
HOMO–5	–6.13	18.9	47.6	30.3	1.7	1.5	d(Ir) + π(C^N)

[a)]bi represents for benzimidazole moiety; [b)]phenyl–1 represents the phenyl group bonded to the Ir atom directly; [c)]phenyl–2 represents the phenyl group bonded to the N atom directly.

Table S5. Frontier molecular orbital energies (eV) and compositions (%) of different fragments for complex **4b** in the ground state, derived from DFT/B3LYP calculations in CH_2C1_2 media.

		Contribution (%)						
MO	Energy(eV)	Ir–d	bi[a)]	phen–1[b)]	phen–2[c)]	*p*–OCH_3	acac	assignment
LUMO+7	0.11	2.0	78	18	1.0	0	0	π*(C^N)
LUMO+3	–0.63	0.5	8.2	1.8	88.2	0.6	0.8	π*(C^N)
LUMO+2	–0.74	2.3	5.5	5.5	0.8	0	87.3	π*(acac)
LUMO+1	–1.26	3.3	58.1	35.2	1.0	0.2	2.2	π*(C^N)
LUMO	–1.32	2.4	57.2	38	0.9	0.3	1.2	π*(C^N)
HOMO	–4.75	43.1	8.3	34	0.2	10.6	3.8	d(Ir) + π(C^N)
HOMO–1	–5.27	45.2	19.3	9.8	0.5	1.1	24	d(Ir) + π(C^N) + π(acac)
HOMO–2	–5.49	6.2	16.2	45.4	0.3	17.7	14.2	π(C^N) + π(acac)
HOMO–3	–5.63	55.5	28.6	10.3	1.0	0.4	4.2	d(Ir) + π(C^N)
HOMO–4	–5.95	8.7	25.5	17.6	0.8	5.2	42.2	π(C^N) +π(acac)
HOMO–5	–6.14	19.1	47.9	29.6	1.3	0.1	2.0	d(Ir) + π(C^N)

[a)]bi represents for benzimidazole moiety; [b)]phenyl–1 represents the phenyl group bonded to the Ir atom directly; [c)]phenyl–2 represents the phenyl group bonded to the N atom directly.

Table S6. Frontier molecular orbital energies (eV) and compositions (%) of different fragments for complex **4c** in the ground state, derived from DFT/B3LYP calculations in CH_2C1_2 media.

		Contribution (%)						
MO	Energy (eV)	Ir–d	bi[a)]	phen–1[b)]	phen–2[c)]	*m*–OCH_3	acac	assignment
LUMO+3	–0.60	0.5	9.8	2.0	86.5	0	1.1	π*(C^N)
LUMO+2	–0.76	2.3	6.1	4.5	1.4	0.1	85.6	π*(acac)
LUMO+1	–1.12	2.7	59.7	28.0	2.3	3.7	3.7	π*(C^N)
LUMO	–1.15	2.2	60.1	30.4	1.6	4.4	1.2	π*(C^N)
HOMO	–5.01	43.6	15.5	34.2	0.2	2.8	3.8	d(Ir) + π(C^N)
HOMO–1	–5.23	37.3	24.9	16.9	0.4	5.5	14.9	d(Ir) + π(C^N)
HOMO–2	–5.54	13.2	22.4	23.2	0.5	8.1	32.6	π(C^N) +π(acac)
HOMO–3	–5.60	43.5	23.9	20.6	0.6	5.5	5.9	d(Ir) + π(C^N)
HOMO–4	–5.88	39.5	23.7	23.0	1.6	10.1	2.1	d(Ir) + π(C^N)
HOMO–5	–6.06	14.3	37.9	7.6	2.7	1.8	35.6	d(Ir) + π(C^N)+ π(acac)

[a)] bi represents for benzimidazole moiety; [b)]phenyl–1 represents the phenyl group bonded to the Ir atom directly; [c)]phenyl–2 represents the phenyl group bonded to the N atom directly.

Table S7. Frontier molecular orbital energies (eV) and compositions (%) of different fragments for complex **4d** in the ground state, derived from DFT/B3LYP calculations in CH_2C1_2 media.

		Contribution (%)						
MO	Energy (eV)	Ir–d	bi[a)]	phen–1[b)]	phen–2[c)]	*p*–CN	acac	assignment
LUMO+3	–0.98	4.0	4.1	23.1	2.0	6.8	59.9	π*(acac) + π*(C^N)
LUMO+2	–1.11	1.8	4.9	66.4	5.2	20.1	1.5	π*(C^N)
LUMO+1	–1.59	3.9	53.1	39.9	1.3	0.1	1.8	π*(C^N)
LUMO	–1.63	3	50.3	43.6	1	0.7	1.4	π*(C^N)
HOMO	–5.49	48.6	12.2	29.3	0.1	4.5	5.3	d(Ir) + π(C^N)
HOMO–1	–5.62	41.7	15.4	4.7	0.5	0	37.7	d(Ir) + π(acac) + π(C^N)
HOMO–2	–6.02	49.3	33.8	10.2	1.2	0.3	5.3	d(Ir) + π(C^N)
HOMO–3	–6.05	3.1	48.8	18.0	0.1	1.1	28.8	π(C^N) + π(acac)
HOMO–4	–6.36	10.5	54.2	14.7	3.3	1.5	15.9	d(Ir) + π(acac) + π(C^N)
HOMO–5	–6.46	14.4	60.3	21.5	1.9	0	1.7	d(Ir) + π(C^N)

[a)]bi represents for benzimidazole moiety; [b)]phenyl–1 represents the phenyl group bonded to the Ir atom directly; [c)]phenyl–2 represents the phenyl group bonded to the N atom directly.

Table S8. Frontier molecular orbital energies (eV) and compositions (%) of different fragments for complex **4e** in the ground state, derived from DFT/B3LYP calculations in CH_2C1_2 media.

		Contribution (%)						
MO	Energy(eV)	Ir–d	bi[a)]	phen–1[b)]	phen–2[c)]	*m*–CN	acac	assignment
LUMO+3	–0.69	0.6	9.1	2.4	87.6	0.2	0.2	π*(C^N)
LUMO+2	–0.94	2.2	5.6	4.1	0.3	0.1	87.7	π*(acac)
LUMO+1	–1.91	3.2	39.9	44.1	0.9	10.9	1.0	π*(C^N)
LUMO	–1.96	2.2	39.1	46.1	0.8	10.9	0.8	π*(C^N)
HOMO	–5.43	52.6	11.3	29.9	0	0.5	5.6	d(Ir) + π(C^N)
HOMO–1	–5.59	43.1	15.0	4.5	0.5	0.4	36.4	d(Ir) + π(acac) + π(C^N)
HOMO–2	–5.97	51.1	32.1	9.8	1.1	0.7	5.2	d(Ir) + π(C^N)
HOMO–3	–6.03	3.1	47.2	17.6	0.1	2.5	29.4	π(C^N) + π(acac)
HOMO–4	–6.34	10.8	53.6	14.4	3.4	1.4	16.4	d(Ir) + π(C^N) + π(acac)
HOMO–5	–6.42	15.3	55.7	22.0	1.8	3.4	1.8	d(Ir) + π(C^N)

[a)]bi represents for benzimidazole moiety; [b)]phenyl–1 represents the phenyl group bonded to the Ir atom directly; [c)]phenyl–2 represents the phenyl group bonded to the N atom directly.

Table S9. Frontier molecular orbital energies (eV) and compositions (%) of different fragments for complex **4f** in the ground state, derived from DFT/B3LYP calculations in CH_2C1_2 media.

		Contribution (%)							
MO	Energy (eV)	Ir–d	bi[a)]	phen–1[b)]	phen–2[c)]	*m*–CN	*p*–OCH_3	acac	assignment
LUMO+3	–0.72	0.5	8.5	2.1	87.9	0	0.6	0.2	π*(C^N)
LUMO+2	–0.90	2.2	5.5	4.3	0.3	0.1	0	87.6	π*(acac)
LUMO+1	–1.90	2.8	40.3	44.1	0.7	10.2	0.8	1.0	π*(C^N)
LUMO	–1.95	2	39.7	45.7	0.7	10.1	1.0	0.7	π*(C^N)
HOMO	–5.13	45.4	7.7	31.9	0.1	0.8	9.6	4.5	d(Ir) + π(C^N)
HOMO–1	–5.52	44.2	15.5	4.9	0.5	0.5	0.1	34.2	d(Ir) + π(acac) + π(C^N)
HOMO–2	–5.87	1.0	28.4	39.9	0.2	4.0	13.0	13.6	π(C^N) + π(acac)
HOMO–3	–5.91	52.9	31.6	9.1	1.1	0.6	0.5	4.3	d(Ir) + π(C^N)
HOMO–4	–6.19	12.9	27.4	17.8	1.5	0.3	6.9	33.2	d(Ir) + π(acac) + π(C^N)
HOMO–5	–6.40	14.8	56.6	21.7	1.5	3.6	1.6	1.8	d(Ir) + π(C^N)

[a)]bi represents for benzimidazole moiety; [b)]phenyl–1 represents the phenyl group bonded to the Ir atom directly; [c)]phenyl–2 represents the phenyl group bonded to the N atom directly.

Table S10. Frontier molecular orbital energies (eV) and compositions (%) of different fragments for complex **4g** in the ground state, derived from DFT/B3LYP calculations in CH_2C1_2 media.

		Contribution (%)							
MO	Energy (eV)	Ir–d	bi[a)]	phen–1[b)]	phen–2[c)]	*p*–CN	*m*–OCH_3	acac	assignment
LUMO+3	–0.95	3.3	4.6	12.9	1.1	2.6	0.7	74.8	π*(acac) + π*(C^N)
LUMO+2	–1.09	2.2	1.9	67.6	5.1	19.3	1.9	1.9	π*(C^N)
LUMO+1	–1.41	2.2	57.3	32.4	1.9	0.1	3.7	2.4	π*(C^N)
LUMO	–1.43	2.7	55.3	34.6	1.4	0	4.8	1.2	π*(C^N)
HOMO	–5.43	41	17	31	0.1	5.0	2.0	4.0	d(Ir) + π(C^N)
HOMO–1	–5.56	39.2	20.8	9.9	0.4	0.3	2.8.	26.6	d(Ir) + π(acac) + π(C^N)
HOMO–2	–5.85	0	29.6	22.5	0.2	2.1	7.8	29.0	π(acac) + π(C^N)
HOMO–3	–5.95	44.0	28.2	16.2	0.8	0.3	3.8	6.7	d(Ir) + π(C^N)
HOMO–4	–6.23	31.1	32.1	22.8	1.8	0	10.0	2.1	d(Ir) + π(C^N)
HOMO–5	–6.28	14.2	47.2	8.0	3.3	1.0	2.1	24.3	d(Ir) + π(acac) + π(C^N)

[a)]bi represents for benzimidazole moiety; [b)]phenyl–1 represents the phenyl group bonded to the Ir atom directly; [c)]phenyl–2 represents the phenyl group bonded to the N atom directly.

References

1 Oxford Diffraction, *CrysAlisPro CCD and CrysAlisPro RED, including ABSPACK*, Oxford Diffraction Ltd, Yarnton, England, 2009.

2 S. L. Mayo, B. D. Olafson and W. A. Goddard, *J. Phys. Chem*., 1990, **94**, 8897–8909.

3 R. E. Stratmann, G. E. Scuseria and M. J. Frisch, *J. Chem. Phys*., 1998, **109**, 8218–8224.

4 P. J. Hay and W. R. Wadt, *J. Chem. Phys*., 1985, **82**, 299–310.

5 M. J. Frisch, G. W. Trucks and H. B. Schlegel, Gaussian 09; Gaussian, Inc.: Wallingford, CT, 2009.

6 E. Cancès, B. Mennucci and J. Tomasi, *J. Chem. Phys*. 1997, **107**, 3032–3041.

7 I.-M. Chan, W.-C. Cheng and F. C. Hong, *Appl. Phys. Lett*., 2002, **80**, 13–15.

8 W.-S. Huang, J. T. Lin, C.-H. Chien, Y.-T. Tao, S.-S. Sun and Y.-S. Wen, *Chem. Mater*., 2004, **16**, 2480–2488.

9 (a) K. Tangdenpaisal, S. Sualek, S. Ruchirawat and P. Ploypradith, *Tetrahedron*, 2009, **65**, 4316–4325; (b) F. Wang, J. A. D. Good, O. Rath, H. Y. K. Kaan, O. B. Sutcliffe, S. P. Mackay and F. Kozielski, *J. Med. Chem*., 2012, **55**, 1511–1525; (c) D. A. Watson, X. Fan and S. L. Buchwald, *J. Org. Chem*., 2008, **73**, 7096–7101; (d) M. Zaheer, M. Zia-Ur-Rehman, S. Rahman, N. Ahmed and M. N. Chaudhary, *J. Chil. Chem. Soc*., 2012, **57**, 1492–1496.

10 D. Wang, L. Kuang, Z. Li and K. Ding, *Synlett*, 2008, **1**, 69–72.

11 Z. Ge, T. Hayakawa, S. Ando, M. Ueda, T. Akiike, H. Miyamoto, T. Kajita and M. Kakimoto, *Chem. Mater*., 2008, **20**, 2532–2537.

12 M. Tavasli, T. N. Moore, Y. Zheng, M. R. Bryce, M. A. Fox, G. C. Griffiths, V. Jankus, H. A. Al-Attar and A. P. Monkman, *J. Mater. Chem*., 2012, **22**, 6419–6428.